https://doi.org/10.5194/egusphere-2023-118
Preprint. Discussion started: 7 March 2023
© Author(s) 2023. CC BY 4.0 License.

Mid-Holocene climate record in Santovka travertine (Slovakia) in context of regional discrepancies of climate shifts 8.2 and 7.4 ka BP

Jan Petřík 1, Katarína Adameková 1, Sándor Kele 2,3, Rastislav Milovský 4, Libor Petr 5, Peter Tóth 6, Nicholas McKay 7

1 Department of Geological Sciences, Faculty of Science, Masaryk University, Kotlářská 2, 611 37 Brno, Czech Republic
2 Institute for Geological and Geochemical Research, Research Centre for Astronomy and Earth Sciences, ELKH, Budapest, Budaörsi út 45., H-1112 Hungary.
3 CSFK, MTA Centre of Excellence, Budapest, Konkoly Thege Miklós út 15-17., H-1121, Hungary
4 Earth Science Institute, Slovak Academy of Sciences, Ďumbierska 1, 97411 Banská Bystrica, Slovakia
5 Department of Botany and Zoology, Faculty of Science, Masaryk University, Kotlářská 2, 611 37 Brno, Czech Republic
6 Department of Archaeology and Museology, Faculty of Arts, Masaryk University, Joštova 220/13, 662 43 Brno, Czech Republic
7 School of Earth and Sustainability, Northern Arizona University, 4099 Flagstaff, AZ 86011, USA

Correspondence to: Jan Petřík (petrik.j@sci.muni.cz)

Abstract

The study of freshwater carbonates, such as travertines and speleothems, provides valuable insights into the regional biases of mid-Holocene climate development in Central-Eastern (CE) and South-Eastern (SE) Europe. The formation of a lake in the travertine deposition system of the Santovka site, located at the transition of the Western Carpathians and the Pannonian Basin, has led to the preservation of a valuable record. We analyzed the litho- and microstratigraphy, chemical composition, including $\delta^{18}O$ and $\delta^{13}C$ stable isotopes, and geochronology of the Santovka-village section. We then compared these palaeoclimatic records with reference records from Central-Eastern and South-Eastern Europe in terms of significant climate shifts. The prevalent part of the section studied, which spans between 8200 and 6400 cal BP, is represented by fluvial/fluvio-lacustrine sediments and lake marl. The 8.2 ka BP event was only detected in the $\delta^{13}C$ record from the nearby Santovka-PB section. However, we found an abrupt change in both isotopic records around 7400–7200 cal BP, which is likely connected to increased detrital input and some minor palaeoecological changes in the Santovka-village section. These changes are most likely associated with the drying of the lake. The 8.2 event in Central-Eastern (CE) and South-Eastern (SE) Europe is well reflected in the $\delta^{13}C$ records, while the change in $\delta^{18}O$ was insignificant. In contrast, the newly suggested climate shift around 7400–7000 ka BP was detected at most sites in both $\delta^{18}O$ and $\delta^{13}C$ records. This development could be connected to a change in air mass circulation, synchronous with declining solar irradiance and increased evidence of drift ice in the North Atlantic.

https://doi.org/10.5194/egusphere-2023-118
Preprint. Discussion started: 7 March 2023
© Author(s) 2023. CC BY 4.0 License.

1. Introduction

The mid-Holocene geological subepoch, formalized as the Northgrippian Age ~ 8.2–4.2 ka BP (e.g. Walker et al., 2018; 2019), started with cold and dry conditions across the Northern Hemisphere (Alley and Ágústsdóttir, 2005; Rohling and Pälike, 2005). Its onset is known as the 8.2 ka BP event and was followed by a return to climatic conditions typical of the Holocene thermal optimum (HCO). The mid-Holocene development varies regionally throughout Europe and is biased by a mismatch between climatic models and proxy records derived mostly from pollen data (c.f. Russo et al., 2022). Correlations of European isotopic speleothem records with climate simulations and sea surface temperature records have demonstrated that not only insolation, but also North Atlantic ocean circulation played a significant role in the sub-millennial variation of continental moisture transport (Demény et al., 2021). This underlines the importance of regional stable isotope studies, which can help to clarify spatial-temporal development of climate dynamics during the mid-Holocene with a focus on $\delta^{18}O$ and $\delta^{13}C$ records.

These records allow us to examine regional discrepancies and point out the influence of Atlantic and continental air flow during the mid-Holocene in Central and Eastern Europe. So far, speleothems have been considered reliable palaeoclimatic archives in the Carpathians (e.g. Drăguşin et al., 2014; Hercman et al., 2020), the Eastern Alps (e.g. Boch et al., 2009) and the northern Balkans (e.g. Tămaş et al., 2005; Surić et al., 2021). Palaeoclimatic investigations in the Western Carpathians and the northern Pannonian basin have been mainly conducted on travertines and tufas (e.g. Demovic et al., 1972; Žák et al., 2001; Dobrowolski et al., 2002; Pazdur et al., 2002; Kele et al., 2006; Gradzinski et al., 2008; Kele, 2009; Demény et al., 2013; Juřičková et al., 2018; Dabkowski et al., 2019; Šolcová et al., 2020; Vieira et al., 2022), as they are abundant in the Central Europe. However, for a robust regional climate reconstruction, more stable isotope analysis from terrestrial carbonate deposits (i.e. travertines and speleothems) are needed. We therefore decided to focus on stable isotope data supplemented with Mg, Sr and Ca element ratios of travertine deposits at Santovka (Slovakia) (Fig. 1). In this study we analyze the sedimentological setting together with extra-sedimentological parameters allowing the classification of deposits (Capezzuoli et al., 2014) prior to the subsequent decoding of geochemical records.

The main aim of this paper is to evaluate validity of the palaeoclimatic record of the Santovka-village sedimentary section, which is part of the Santovka travertine deposit system, and to compare it with other high-resolution palaeoclimatic and chronostratigraphic records. This will be achieved by (1) a detailed characterization of the site formation processes and depositional environment, by (2) a reconstruction of the palaeoclimatic conditions based on the $\delta^{18}O$, $\delta^{13}C$ and element data combined with an enhanced age-depth model, and by (3) a spatio-temporal comparison of climate shifts in relevant published climatic records.

https://doi.org/10.5194/egusphere-2023-118
Preprint. Discussion started: 7 March 2023
© Author(s) 2023. CC BY 4.0 License.

2. Regional setting

The Santovka site is located about 120 km east of Bratislava (Slovakia) at the transition of the Carpathians (Slovak Central Mountains) and the Pannonian Basin, within which it belongs to the Danubian Hills (Fig. 1; Mazúr and Lukniš, 1986). The climate is warm and dry with mild winters (climatic zone T2), with a mean annual temperature of 8–9 °C and mean annual precipitation of 550–600 mm (Miclós, 2002), and its mean annual $\delta^{18}O$ value varies around −9.19 ‰ (station Mochovce, Holko et al., 2012). The surroundings of Santovka are built of freshwater limestones of Late Pleistocene to Holocene age, classified as travertine spring mounds and fissure ridges (Pivko and Vojko, 2021). The travertine mounds are linked to the discharge of groundwater with sufficiently deep circulation in an environment of calcium-rich rocks. Their emergence and occurrence is controlled by the activity of extensional fault structures (Hók et al., 2020). The related presence of thermal and mineral springs at Santovka is linked to mineral waters of the 'Levice Spring Line' (Bačová et al., 2016). Aquifers of mineral and thermal waters of deep origin are mainly formed in Mesozoic limestones and dolomites in the Inner Carpathians (Vieira et al., 2022**)**. Recently, the temperature of the springs has ranged from 12 °C (cores B-15 and B-6) to 26.6 °C (core B-3A; Franko et al., 1995; Bačová et al., 2015). In the wider area of the Santovka site, there are neovolcanites represented mainly by pyroxenic andesite tuffs and tuffitic sandstones of andesites (Konečný, 1998). Besides travertines, the quaternary deposits consist of loess, loess-like sediments, and fluvial and deluvial sediments (Maglay et al., 2009).

At the site, two sedimentary sections have so far been examined in terms of environmental changes: Santovka-village and Santovka-Pramene Budzgov (PB) (Fig. 1). The subject of this research, an outcrop known as Santovka-village (48.1538958N, 18.7691178E) currently forms the right bank of the Búr brook (Fig. 2). The section is located at an elevation of 140 m asl and it is formed mainly by organic-rich carbonate sediments (Fig. 2) bearing prehistoric ceramics (Šolcová et al., 2018). The nearest spring (core B-3A), situated circa 100 m from the section, is classified as thermal with a temperature of 26.6 °C and and has a yield of 8 l/s (Franko et al., 1995; Bačová et al., 2015).

https://doi.org/10.5194/egusphere-2023-118
Preprint. Discussion started: 7 March 2023
© Author(s) 2023. CC BY 4.0 License.

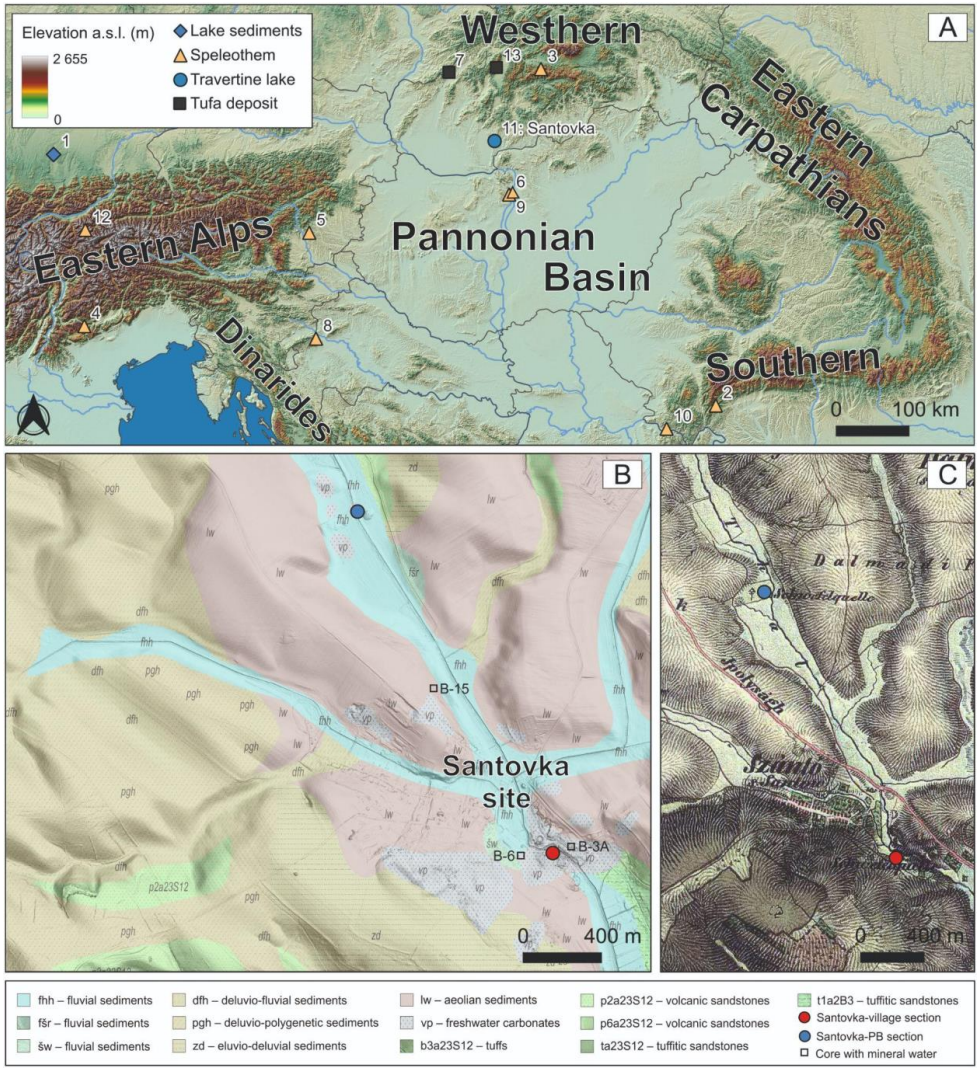

Fig. 1 A – Position of the area of interest within Europe, with selected $\delta^{18}O$ and $\delta^{13}C$ records (1: Ammersee; 2: Ascunsă Cave POM2; 3: Demänovská Cave HcH2A; 4: Grotta di Ernesto Cave ER 76; 5: Katerloch Cave K1; 6: Leány; 7: Mituchovci; 8: Nova Grgosova Cave NG-3; 9: Pál-völgyi Cave; 10: Poleva Cave; 11: Santovka-village and Santovka-PB; 12: Spannagel Cave; 13: Valča) (CGIAR CSI, 2023; Natural Earth Data, 2023). B – Geological map of the surroundings of the Santovka site, with the position of the section Santovka-village under study and those of the nearest section Santovka-PB (Šolcová et al., 2020) and recent hydrogeological cores with mineral water (Bačová et al., 2015). Terrain morphology is illustrated by the hill shade layer (SGUDS, 2023; ZBGIS, 2023). C – Historical map (1819–1869) adapted from the second Austro-Hungarian military survey (Maps Arcanum, 2023)

https://doi.org/10.5194/egusphere-2023-118
Preprint. Discussion started: 7 March 2023
© Author(s) 2023. CC BY 4.0 License.

Fig. 2 Photograph of the Santovka-village section studied, located on the right bank of the Búr brook, with marked boundaries of lithostratigraphic units (black lines). The positions of sampled log (yellow dashed line) and collected micromorphological samples (yellow rectangles) are indicated. Unit 6b was captured in the core and is not visible in the photograph.

3. Material and methods

The approximately 3 m thick stratigraphic section (Fig. 2) was cleaned, documented and sampled in 2012–2014. Lithostratigraphic units were adapted according to field observations and the palaeoecological study of Šolcová et al. (2018). Bulk samples of carbonate-rich sediment taken at 3-cm and 5-cm resolution have already been evaluated by Šolcová et al. (2018), where the field methodology is described in detail. We revised the same samples in terms of geochemical analyses to obtain concentrations of missing chemical elements. Moreover, carbonate concretions from the same bulk sediment samples were separated by flotation and sieving and manually collected from the wet-sieved material for the purpose of this study. Five additional undisturbed blocks of sediment were collected in the field and were subsequently thin sectioned by drying, impregnation, cutting into slices, fixing on a glass slide and polishing to the thickness of about 30 μm. Micromorphological analysis was performed by a polarizing microscope in transmitted polarized light (PPL) and in cross-polarized light (XPL) at 40×–400× magnifications. Description was conducted according to Stoops (2003). Photographic documentation was performed using a flatbed scanner in PPL at 3200-dpi resolution (Fig. 3A, B).

Chemical analyses of 40 bulk samples of carbonate-rich sediment were performed in a helium

https://doi.org/10.5194/egusphere-2023-118
Preprint. Discussion started: 7 March 2023
© Author(s) 2023. CC BY 4.0 License.

atmosphere using a Rigaku NexCG ED-XRF spectrometer with a 50-W Pd tube with an SSD detector of 145-eV resolution and indirect excitation by secondary targets. Samples were dried and cleaned of stones and organic residues. The samples were homogenized and powdered in a RETSCH PM 100 planetary ball mill, pressed into pellets and finally analysed. The duration of each measurement was 120 s for each secondary target. Matrix-matched calibration was carried out according to international reference materials as well as using internal standards (for details about the reference materials, see Adameková and Petřík, 2022). Only concentrations for the elements Mg, Al, Si, S, K, Ca, Ti, Mn, Fe, Rb and Sr are discussed.

Stable carbon and oxygen isotopes were analysed on 23 bulk carbonate concretions by an isotope-ratio mass spectrometer (IRMS) MAT253 (ThermoScientific) at the Slovak Academy of Sciences in Banská Bystrica (Slovakia). Pulverized samples were loaded into borosilicate glass vials, flushed with helium to remove the atmosphere and digested overnight in 103% phosphoric acid (McCrea 1950) at 40°C. The evolved CO_2 was analysed using a Gasbench III device coupled in continuous-flow mode to IRMS. The isotope values were calibrated using two standards traceable through international reference materials (NBS18, NBS19) to the PDB scale. Results are reported in per mill vs PDB; the external standard deviation is 0.18 and 0.09 permil for $\delta^{18}O$ and $\delta^{13}C$, respectively.

The geochronology is based on four dates adapted from Šolcová et al. (2018) supplemented by six new radiocarbon dates: three for bones and three for wood. Radiocarbon dating was performed in the Center for Applied Isotope Studies at University of Georgia (UGAMS) with acid-alkali-acid (AAA) pretreatment. An enhanced age-depth model was created using the GeochronR 1.1.9 library (McKay et al., 2021) with the runBacon function based on the rBacon package (Blaauw et al., 2022) according to the Intcal20 calibration curve (Reimer et al., 2020). Subsequently, accumulation rates were calculated for lithostratigraphic boundaries by the accrate.depth function of the rBacon package. The age of individual bulk samples containing carbonate concretions bearing isotopic record was derived from mean age values of specific depths obtained by the runBacon function. The obtained mean age was added to a LiPD file used by GeochronR to plot isotopic curves.

The age–depth model was also used for the age-ensembling of geochemical and isotopic records (Appendix). Isotopic records of $\delta^{18}O$ and $\delta^{13}C$ from the Santovka site, together with records from relevant speleothems, travertines and tufas from Central-Eastern and South-Eastern Europe (Fig. 1), were compiled into LiPD (McKay et al., 2016) files and age-ensembled. Regional records were selected according to time span, age, record resolution, geographic position and data availability. All sites from continental Europe were located between 44.7144N to 49.0010556N and 11.1167E to 22.6E. The nearest comparable $\delta^{18}O$ records outside the Western Carpathians originate from speleothems found in the Eastern Alps (Boch et al., 2009; Scholz et al., 2012; Fohlmeister et al., 2013), the northern Balkans (Surić et al. 2021), the Eastern and the Southern Carpathians (cf. Constantin et al., 2007; Drăguşin et al., 2014), and the Pannonian Basin (Demény et al., 2013). One $\delta^{18}O$ record originate from the lake in pre-alpine region of southern Germany (Czymzik et al., 2013). NGRIP $\delta^{18}O$ record originating from

https://doi.org/10.5194/egusphere-2023-118
Preprint. Discussion started: 7 March 2023
© Author(s) 2023. CC BY 4.0 License.

Greenland glacier (NGRIP Members, 2004) was included to illustrate the presence of the 8.2 ka BP event. Selected records were analysed by the actR package (McKay et al., 2022) designed for abrupt change detection, significance testing, uncertainty quantification and visualization of palaeogeoscientific datasets. The detectShift function was used within an optimal time window between the lowest age of 8700 cal BP (similarly to the work of Weninger et al. 2006) and 6400 cal BP (the youngest reliable period recorded in Santovka-village) to infer the probability of climatic shifts in mean results, which were significant at the $\alpha < 0.05$ level. Consequently, we compared spatio-temporal patterns of climate shifts. The R code of procedure is available as Appendix.

4. Results

4.1 Litho- and microstratigraphy

Ten lithostratigraphic units were recognized in Santovka-village sequence from the depth of 275 cm to the present-day surface (Table 1). Only seven units (6b–2c) belong to the part of interest (Fig. 2). The lowermost units (6b and 6a) were composed of heterogeneous very dark greyish brown to dark yellowish brown sandy silt with predominant silicate minerals (mostly quartz, feldspar and mica) mixed with various rounded and angular micritic and sparitic carbonate clasts as well as organic matter remains (Fig. 3C). Units differed mainly in the number of mollusc shells and plant remains (Table S1). The microstructure of unit 6b was described as massive because of a scant presence of voids (locally channels and plane voids). Striated b-fabric predominated and a crystallitic b-fabric occurred locally. Fine organic matter was frequent. Redoximorphic iron or manganese nodules occurred rarely. Charcoals and fragments of bone were also present (Fig. 3C, D).

The 5b and 5a units were composed mostly of precipitated carbonates, benthic organism remains (mainly diatoms), and, rarely, rounded and angular micritic and sparitic carbonate clasts and fragments of mollusc shells (Fig. 3E, F). The upper unit (5a) differed from the lower (5b) mainly in colour. Unit 5b was of brown colour whereas unit 5a was more greyish brown (Table S1). Unit 5a contained archaeological finds. The microstructure of unit 5a was platy with predominant plane, channel and vugh voids. The B-fabric was crystallitic because of the calcite-rich micromass. Plant tissues and fine organic matter were common. The sediment also contained horizontally lying plant remains (possibly leaves; Fig. 3E) and was locally bioturbated. Charcoal and bone fragments occurred occasionally in the sediment.

A macroscopically significant organic layer, unit 4, is formed by microscopic black organic and very dark greyish brown calcareous laminae and frequent fragments of mollusc shells (Fig. 3G–J). The microstructure of this unit was described as platy with predominant plane and channel voids. It was disturbed by intensive bioturbation. Diatoms occurred frequently and ostracods less often (Table S1). Organic laminae were composed mostly of decomposed organic matter, while calcareous laminae were formed mostly by micritic carbonate concretions and less by organic remains. That is why organic

https://doi.org/10.5194/egusphere-2023-118
Preprint. Discussion started: 7 March 2023
© Author(s) 2023. CC BY 4.0 License.

laminae have undifferentiated b-fabric and those that are carbonated mainly occur mainly with crystallitic b-fabric. The sequence of laminae terminated by a thick organic lamina on which the following lithostratigraphic unit was deposited. This lamina differed slightly from other organic laminae because of a greater amount of organic matter and scarce presence of benthic organisms (Table S1).

Unit 3 consisted of dark greyish brown calcareous sediment composed of benthic organism remains, rounded and angular micritic and sparitic carbonate clasts, and fragmented organic matter. Unit 3 differed from the upper lacustrine sediment in its low degree of compaction and species representation of benthic organisms (ostracods prevailing over diatoms; Table S1). Newly appearing here were elongated calcareous fragments of various sizes formed by micrite and microsparit (Fig. 3K, L), so-called calcite rafts (c.f. Jones, 1989). Calcite rafts used to precipitate on the surface of the water as thin films and then fragmented and sank to the bottom. Microstructure of unit 3 was described as a massive with local occurrence of channel, vugh and plane voids. Local traces of meso- and macrofauna bioturbation were visible. Fragments of bones and also charcoal were present.

The uppermost studied unit 2c was composed of organic-rich clayed unsorted heterogeneous very dark grey sediment. There were frequent fragments of mollusc shells and occasionally fragments of travertines. This unit was not sampled for the purpose of micromorphological analysis.

Table 1 Lithostratigraphic characterization of the Santovka-village section partially adapted by Šolcová et al. (2018).

Unit	Depth [cm]	Description	Interpretation
1	0–48	Dark brown (7.5YR 3/2) sandy loam, intensively rooted, with non-oriented fragments of travertine (ca 30%)	Holocene soil
2a	48–90	Very dark grey (7.5YR 3/1) clayey loam, rooted, with a high proportion (ca 70–80%) of parallel oriented travertine fragments (size 0.5–15 cm) and with shells of mollusc	Colluvium
2b	90–115	Very dark greyish brown (10YR 3/2) sandy clay with frequent shells of molluscs and rarely with travertine fragments (< 1%)	Colluvium
2c	115–139	Very dark grey (10YR 3/1) organic-rich clay with frequent shells of mollusc shells; travertine fragments (< 5%) and travertine layer (in depth of 125–131 cm)	Colluvium

https://doi.org/10.5194/egusphere-2023-118
Preprint. Discussion started: 7 March 2023
© Author(s) 2023. CC BY 4.0 License.

3	139–149	Dark greyish brown (10YR 4/2) organic-rich calcareous sediment	Lake marl
4	149–152	Organic layer composed of black (10YR 2/1) organic-rich and very dark greyish brown (10YR 3/2) calcareous laminae	Organic sediment with with biochemical calcite laminae
5a	152–186	Greyish brown (10YR 5/2) calcareous sediment, weakly bioturbated, travertine fragments (< 5%, 178–180 cm)	Lake marl
5b	186–204	Brown (10YR 4/3) calcareous sediment, weakly bioturbated, travertine layer (198 cm)	Lake marl
6a	204–215	Dark yellowish brown (10YR 3/4) organic-rich sediment of heterogeneous character, silicate minerals mixed with angular to surrounded fragments of travertines as well as of partially and completely decomposed organic matter and rare charcoals	Fluvial/fluvio-lacustrine sediments
6b	215–275	Very dark greyish brown (10YR 3/2) organic-rich sediment of heterogeneous character with molluscs and plant remains, silicate minerals mixed with angular to surrounded fragments of travertines as well as of partially and completely decomposed organic matter and rare charcoals	Fluvial/fluvio-lacustrine sediments

https://doi.org/10.5194/egusphere-2023-118
Preprint. Discussion started: 7 March 2023
© Author(s) 2023. CC BY 4.0 License.

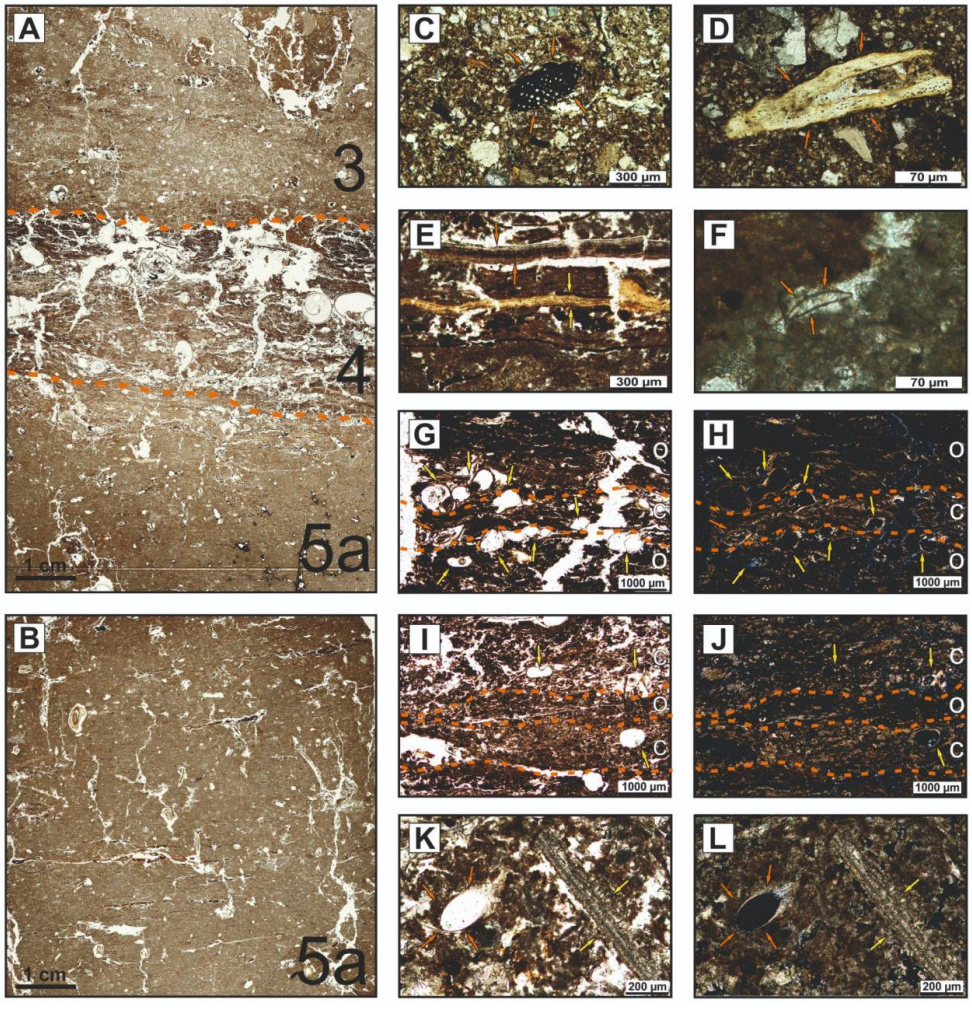

Fig. 3 Photographs of thin sections and microphotographs of selected features in transmitted polarized light (PPL) and in cross-polarized light (XPL). The locations of collected samples are shown in Fig. 2. **A** – Scan of sample 1 which captures partially units 3 and 5a and the whole unit 4. The boundaries between the individual units are indicated by the orange dashed line. **B** – Scan of thin section 2 which represents unit 5a. **C** – Matrix composed of sandy silt with predominant silicate minerals mixed with organic matter remains, charcoal (orange arrows), unit 6b (PPL). **D** – Matrix composed of sandy silt with predominant silicate minerals mixed with organic matter remains, bone fragment (orange arrows), unit 6b (PPL). **E** – Mollusc shell (orange arrows), horizontally lying organic matter remains, possibly leaves (yellow arrows), highly calcareous matrix, unit 5a (PPL). **F** – Highly calcareous matrix with diatoms (orange arrows), unit 5a (PPL). **G** – Organic (o) and calcareous (c) laminae whose boundaries are indicated by the orange dashed line, mollusc shells (yellow arrows), unit 4 (PPL). **H** – Analogical case as in Fig. 3G (XPL). **I** – Organic (o) and calcareous (c) laminae whose boundaries are indicated

https://doi.org/10.5194/egusphere-2023-118
Preprint. Discussion started: 7 March 2023
© Author(s) 2023. CC BY 4.0 License.

by the orange dashed line, mollusc shells (yellow arrows), unit 4 (PPL). **J** – Analogical case as in Fig. 3I (XPL). **K** – Bivalvia (orange arrows) and raft (yellow arrows), unit 3 (PPL). **L** – Analogical case as in Fig. 3K (XPL).

4.2 Chemical composition and stable isotopes

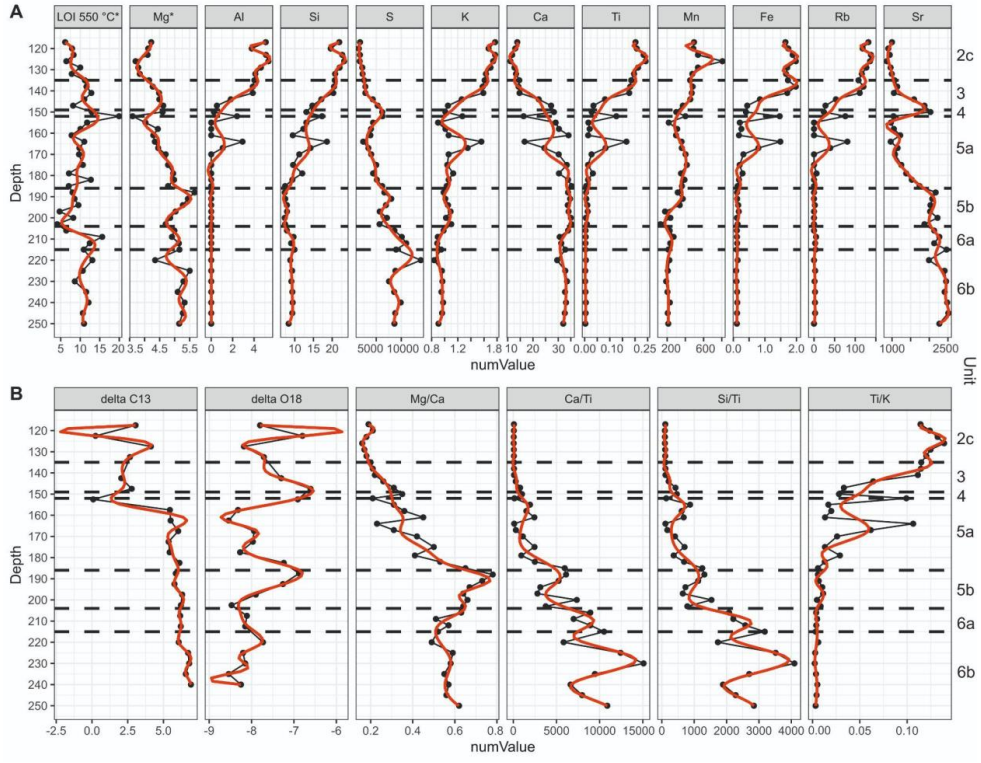

Fig. 4 Concentration of chemical elements (A), stable isotope values and elemental ratios (B) at particular depths and in specific units (black dots and line), with a smoothed line produced by the spline function (red). Values with * were adapted from Šolcová et al. (2018).

Relations of elements (expressed in ppm) vary across depths and lithostratigraphic units (Fig. 4 and Appendix). Lowermost units 6b and 6a (275–204 cm) bear relatively high S (7,550–13,900) values associated with increased LOI (~ 6.4–15.6% organics) as well as Ca (296,000–339,000), Mg (4.3–5.1) and Sr (1990–2510) values, while Si (79,000–99,200), Ti (22.2–50.8), Mn (189–270, dipping to 126 at 203 cm), Fe (910–1,360) and Rb (0–5.0) are low compared to other units. Units 5b and 5a (204–152 cm) has lower LOI values (~ 4.1–12.7% organics) and decreasing concentrations of S (to 2380), while Mg (4.0–5.6), Ca (167,000–353,000) and Sr (971–2,220) are relatively high up to 5b/5a boundary and then decrease in unit 5a. Values of Si (73,000–186,000), Ti (47.6–1,660), Al (73,000–186,000), Fe (1,120–

https://doi.org/10.5194/egusphere-2023-118
Preprint. Discussion started: 7 March 2023
© Author(s) 2023. CC BY 4.0 License.

14,900) and Rb (0–81) are lower in units 5a and 5b, with an abrupt peak at 167–164 cm. Values of Mn (126–416) increase slightly in unit 5b and decrease in the upper part of unit 5a. The change is clearly visible in unit 4 (152–149 cm), where at the bottom abruptly increase LOI values up to ~ 19.9 % organics as well as S (to 6250), Si (to 173,000), Ti (to 1,260), Mn (to 400), Fe (to 14,700) and Rb (to 75.9), while Ca (163,000), Mg (3.6) and Sr (1,040) decrease at the bottom and increased at the top (149 cm). Unit 3 (149–139 cm) has similar values of LOI (~8.1–12.8 % organics) and S (5,280–2,820) as unit 5a, while Ca (to 147,000), Mg (to 4.4) and Sr (to 1,050) decrease and Al (5,280–38,800), Si (147,000–203,000) and Ti (348–1,770) with Mn (372–470), Fe (4,400–17,100) and Rb (27.8–111) increase. This trend graduate in unit 2c, where Al (232,000), Si (203,000), Ti (232,000), Mn (807) and Fe (19800) reach maximum, while LOI (to 6.1 % organics), S (to 1,510), Ca (to 111,000), Mg (to 3.7) and Sr (to 861) significantly decrease.

Values of Mg/Ca are increasing in units 6a–5b with maximum at the depth of 188 cm (0.78) and then the overall trend decreasing towards the top of the section with local minimums at 164 cm (0.23) and 152 cm (0.21). Significant local maximums are at 161 cm (0.45) and 150 cm (0.35). Both Ca/Ti and Si/Ti ratios have similar trends with big magnitude of generally high values in units 6b–6a (up to 15090 for Ca/Ti and 4094 for Si/Ti) and generally decreasing values through unit 5b and 5a to local minimums in 164 cm (100 for Ca/Ti and 112 for Si/Ti) and in the depth of 152 cm (129 for Ca/Ti and 137 for Si/Ti). A little increased values in unit 4 (up to 1000 for Ca/Ti and 464 for Si/Ti) are followed by a decrease and very low values in units 3 (to 79 Ca/Ti and to 113 Si/Ti) and 2c (to 50 Ca/Ti and to 94 Si/Ti). Curves of Ti/K and Mg/Ca have the opposite trend to Ca/Ti and Si/Ti.

Values of $\delta^{18}O$ in Santovka-village section (Fig. 5) range between −8.5 and −6.6 ‰ (−7.8‰ average). Significantly low values (−8.5 to −7.7‰) were detected at the bottom at depths of about 240–200 cm in unit 6b (Fig. 4), followed by increasing values (−7.9 to −6.8‰) between 200–185 cm in unit 5b. A clearly visible decrease (up to −8.5 ‰) between 185 and 155 cm in unit 5a is followed by an abrupt increase in values (−6.9 ‰) around 155–150 cm at the transition of units 5a and 4. Subsequently, values in unit 3 and 2c decrease again up to −8.1‰ at 125 cm. Values of $\delta^{13}C$ (Fig. 5) have quite a wide range from ca 0.1 to 6.9‰ (4.9‰ on average), but do not oscillate so much between 240 and 155 cm (6.9–5.3‰) in units 6b–5a (Fig. 4, Appendix). An abrupt decrease (to ca 0.1‰) comes between 155 and 150 cm at the boundary of units 5a and 4, followed by a minor increase (to 4.1 ‰) between 150 and 130 cm in unit 3 and partially in unit 2c. The second abrupt decrease (0.2‰) in 125 cm was captured in unit 2c.

https://doi.org/10.5194/egusphere-2023-118
Preprint. Discussion started: 7 March 2023
© Author(s) 2023. CC BY 4.0 License.

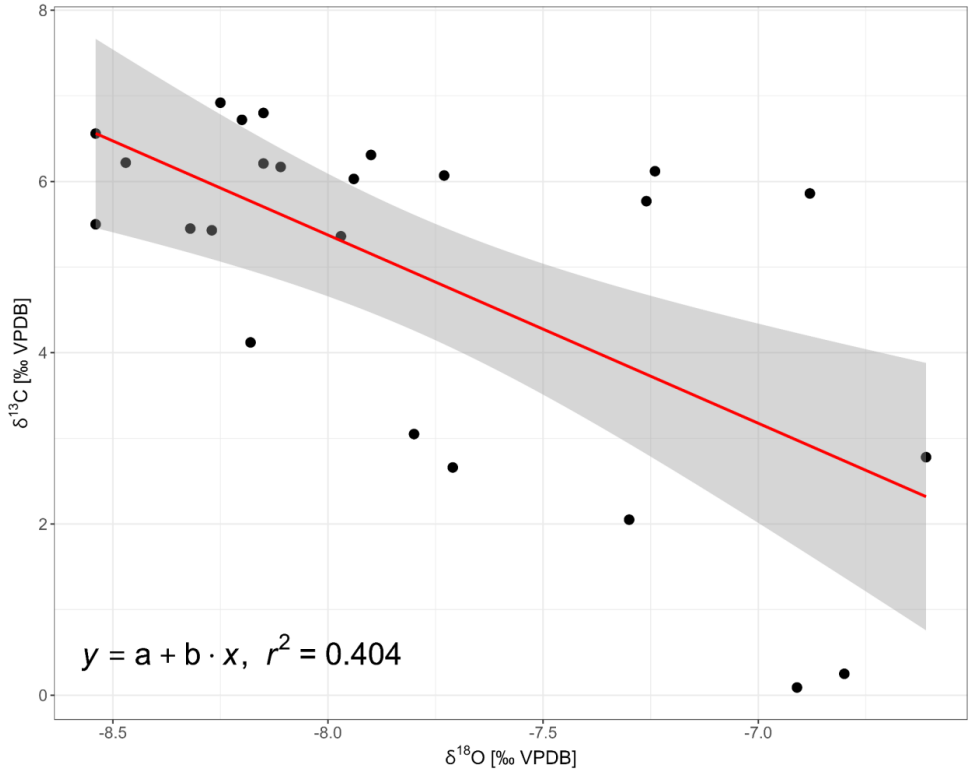

290 **Fig. 5** Comparison of $\delta^{18}O$ and $\delta^{13}C$ isotopes derived from carbonate concretions from the Santovka-village section.

4.3 Geochronology and accumulation rates

Nine of ten radiocarbon ages (Table 2) were used to build the age–depth model (Appendix, Fig. 6) with a time span of 8200 to 6400 cal BP. The sample UGAMS 19700 (fishbone) was avoided due to a
295 possible reservoir effect. The age obtained from sample UGAMS 10046 was included into the age-depth model but not projected (Fig. 6). We set boundaries at the depths of 204 (units 6a/5b), 149 (units 4/3) and 139 cm (units 3/2), assuming a change in the sedimentary environment and deposition rate. The mean accumulation rate is 12.7 yr/cm; however, there are differences in accumulation rates in particular units (Fig. 6; Appendix). Unit 6b accumulated till no later than ~8100 cal BP with an
300 accumulation rate of 3.7–10.3 yr/cm and unit 6a till ~8050 cal BP with an accumulation rate values of 3.5–4.1 yr/cm. Unit 5b accumulated till ~7900 cal BP, when unit 5a started to accumulate. Its sedimentation finished ~7300 cal BP. The values of accumulation rates are 4.0–8.5 yr/cm for unit 5b and are decelerated in unit 5a with values of 7.2–24.5 yr/cm. Unit 4 accumulated during a short period till no later than ~7200 cal BP with a sediment accumulation rate of 13.3–16.7 yr/cm. Overlying unit 3
305 accumulated between ~7200 and ~6900 cal BP and unit 2c from ~6900 cal BP onward. The

https://doi.org/10.5194/egusphere-2023-118
Preprint. Discussion started: 7 March 2023
© Author(s) 2023. CC BY 4.0 License.

accumulation rate decelerated in unit 3 (5.6–126.3 yr/cm) and accelerated in unit 2c (5.4–34.9 yr/cm).

Table 2 Results of radiocarbon dating of new samples together with four dates adopted from Šolcová et al. (2018) used for age-depth modeling.

Laboratory number	**Sample name**	**Material**	**Depth (cm)**	**Unit**	**Radiocarbon age (yr. BP)**	**References**
UGAMS 10043		Charcoal	130	2c	5730±25	Šolcová et al., 2018
UGAMS 52963	Bone 8	Animal bone (cervical vertebrae from a horse)	144	3	6050 ± 25	this paper
UGAMS 53825	Wood 3	Wood	149	4	6510 ± 50	this paper
UGAMS 52962	Bone 4	Animal bone (larger bird without further possible specification)	156	5a	6440 ± 30	this paper
UGAMS 19700		Fishbone	175.5	5a	6780±30	this paper
UGAMS 53824	Wood 1	Wood	180	5a	7100 ± 30	this paper
UGAMS 53467	Wood 2	Wood	202	5b	7570 ± 30	this paper
UGAMS 10044		Bark and wood	215	6a/6b	7300±30	Šolcová et al., 2018
UGAMS 10045		Tree buds	270	6b	7400±30	Šolcová et al., 2018
UGAMS 10046		Hazelnut	380		8360±30	Šolcová et al., 2018

310

https://doi.org/10.5194/egusphere-2023-118
Preprint. Discussion started: 7 March 2023
© Author(s) 2023. CC BY 4.0 License.

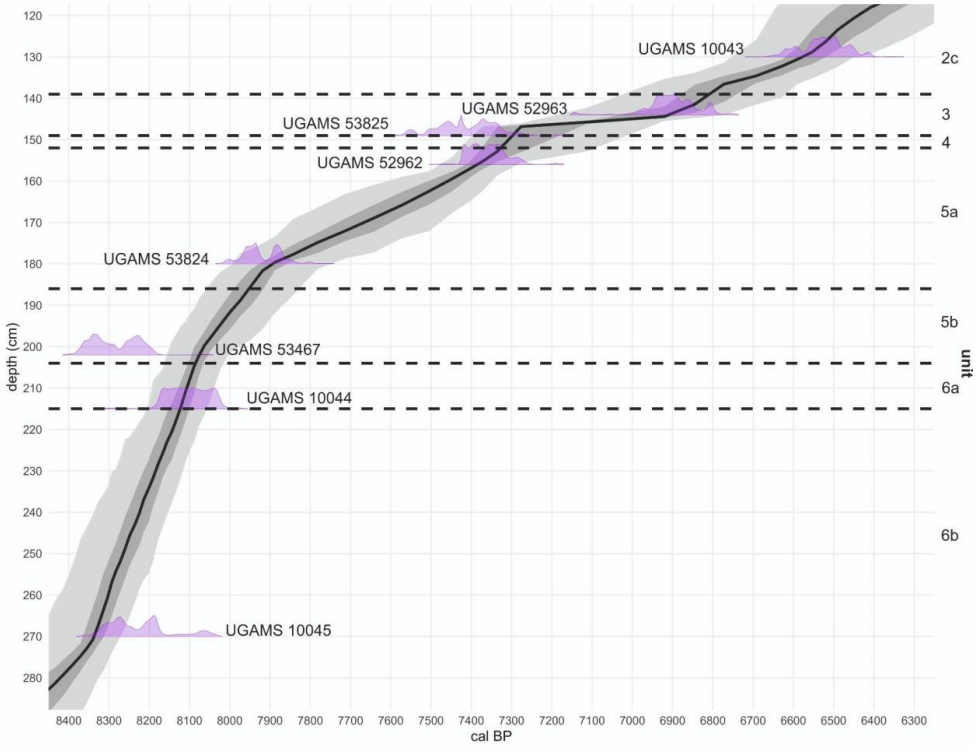

Fig. 6 Age–depth model generated by Bacon from nine radiocarbon ages. Relative age probability distributions are shown in purple. The median age–depth relationship is in black, with 50th and 95th percentile highest-density probability ranges shown in dark and light grey.

https://doi.org/10.5194/egusphere-2023-118
Preprint. Discussion started: 7 March 2023
© Author(s) 2023. CC BY 4.0 License.

4.4 $\delta^{18}O$ and $\delta^{13}C$ stable isotope records and climate shifts

Mean lines of the Santovka-village section indicate a general increasing $\delta^{18}O$ trend, while the $\delta^{13}C$ trend is the opposite (Fig. 7). Four mean shifts for $\delta^{18}O$ were detected with significant probability ($p < 0.001$) for periods between 7404 and 7204 BP. The most significant shift belongs to the period 7404–7354 BP ($p = 0.045$). Only one shift belonging to the period 7304–7254 ($p = 0.04$) was detected for $\delta^{13}C$. No clear pattern was detected in $\delta^{18}O$ shifts of Central-Eastern and South-Eastern Europeean records (Table 3, Appendix). Most of the recognized climate shifts, detected in other inspected archives in both $\delta^{18}O$ and $\delta^{13}C$ records, belong mostly to the periods ~ 8400–7900 and 7500–7200 cal BP (Table 3, Appendix).

https://doi.org/10.5194/egusphere-2023-118
Preprint. Discussion started: 7 March 2023
© Author(s) 2023. CC BY 4.0 License.

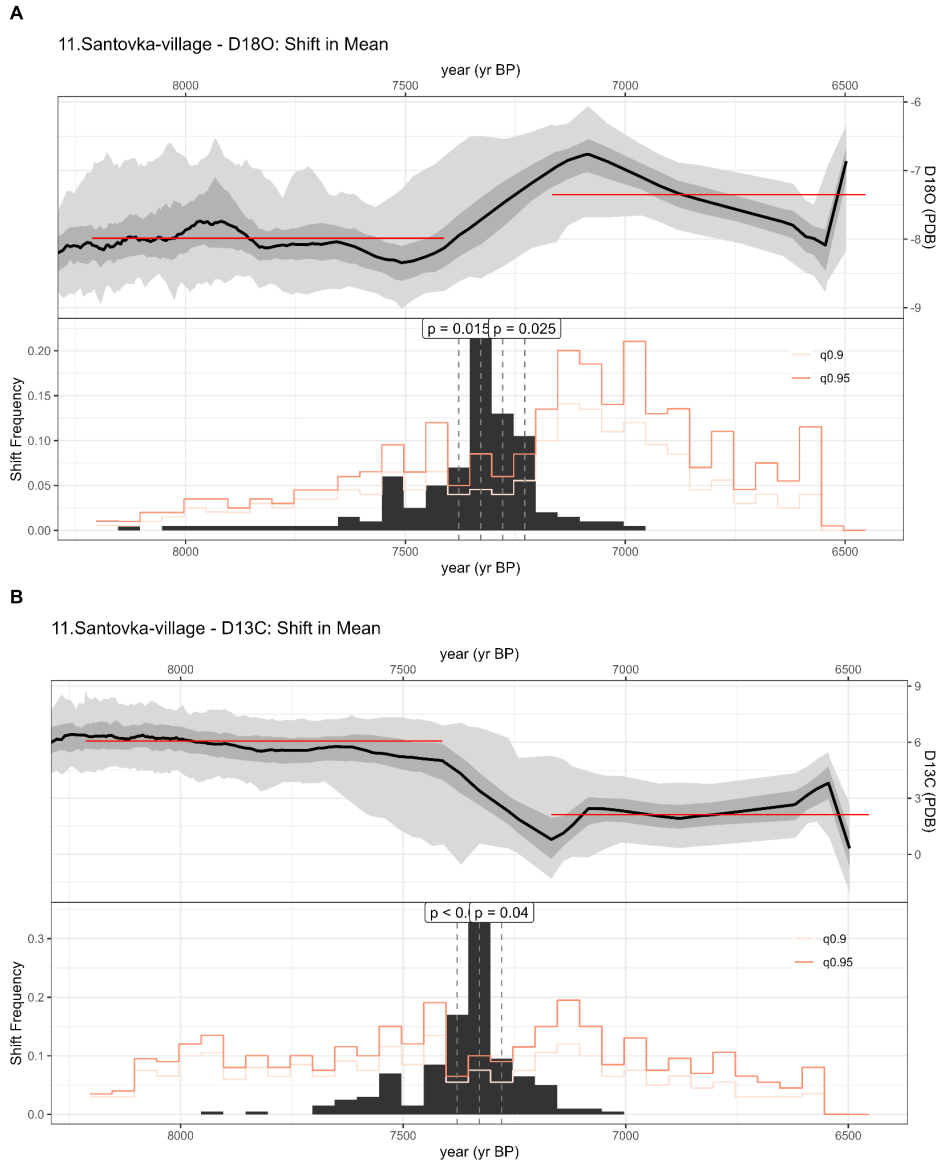

Fig. 7 Time series plot of the $\delta^{18}O$ (A) and $\delta^{13}C$ (B) records of the Santovka-village section with a ribbon of confidence intervals, indicating detected shifts with uncertainties and null hypothesis testing.

340

Table 3 Summary of shift-outs with detected shifts in 50 years steps (cal years BP), with probabilities in brackets. NAs means missing data, – denotes zero detected shifts.

Site and reference	**Archive type**	**Subregion**	**Detected climate shifts** $\delta^{18}O$	**Detected climate shifts** $\delta^{13}C$

https://doi.org/10.5194/egusphere-2023-118
Preprint. Discussion started: 7 March 2023
© Author(s) 2023. CC BY 4.0 License.

Ammersee (Czymzik et al., 2013)	Lake sediment	pre-alpine region (Bavaria)	8115–8065 (0.035)	NA
Ascunsă POM 2 (Drăguşin et al., 2014)	Speleothem	Southern Carpathians	8003–7953 (0.030) 7953–7903 (0.030) 7903–7853 (0.040)	8353–8303 (0.035) 7853–7803 (0.020)
Demänovská Cave HcH2A (Hercman et al., 2020)	Speleothem	Western Carpathians	7757–7707 (0.020) 7707–7657 (0.035) 7657–7607 (0.045)	–
Grotta di Ernesto ER 76 (Scholz et al., 2012)			7252–7202 (0.020)	7402–7352 (0.045)
Katerloch K1 (Boch et al., 2009)	Speleothem	Eastern Alps	7680–7630 (0.040)	7580–7530 (0.020) 7530–7480 (0.025)
Leány (Demény et al., 2013)	Speleothem	Pannonian basin	–	8340–8290 (0.015) 8290–8240 (0.015) 8440–8390 (0.025) 8390–8340 (0.025) 8240–8190 (0.030) 8190–8140 (0.040) 8540–8490 (0.045)
Mituchovci (Dabkowski et al., 2019)	Tufa	Western Carpathians	–	–
Nova Grgosova Cave NG-3 (Surić et al., 2021)	Speleothem	Dinarides	8508–8458 (0.040)	7458–7408 (0.020)
Pál-völgyi (Demény et al., 2013)	Speleothem	Pannonian basin	7763–7813 (0.045) 7313–7263 (0.030)	8463–8413 (0.015) 8413–8363 (0.005) 8363–8313 (0.020) 8313–8263 (0.020) 8263–8213 (0.045)
Poleva Cave (Constantin et al., 2007)	Speleothem	Southern Carpathians	8260–8210 (0.040) 8210–8160 (0.005) 8160–8110 (0.020) 8010–7960 (0.020) 7960–7910 (0.020)	7610–7560 (0.005) 7510–7460 (0.010) 7460–7410 (0.045)
Santovka-village	Travertine lake sediment	Pannonian basin	7404–7354 (0.045) 7354–7304 (0.005) 7304–7254 (0.010) 7254–7204 (0.020)	7304–7254 (0.040)
Santovka-PB (Šolcová et al., 2020)	Travertine lake sediment	Pannonian basin	–	8412–8362 (0.020) 8312–8262 (0.005)
Spannagel Cave (Fohlmeister et al., 2013)	Speleothem	Eastern Alps	7551–7501 (0.010) 7501–7451 (0.020)	NA
Valča (Juřičková et al., 2018)	Tufa	Western Carpathians	–	7709–7659 (0.015) 7659–7609 (0.025)
NGRIP (NGRIP Members, 2004	Glacier ice	Greenland	8110–8060 (0.030)	NA

https://doi.org/10.5194/egusphere-2023-118
Preprint. Discussion started: 7 March 2023
© Author(s) 2023. CC BY 4.0 License.

5. Discussion

5.1 Sedimentary history (site formation/depositional processes)

The valley bottom of Búr brook at the Santovka site was originally infilled with fluvial/fluvio-lacustrine sediments (units 6b and 6a) deposited by the local stream before ~ 8050 cal BP (boundary unit 6a/5b). The chemical composition of these sediments reflects an environment with high production of organics (high LOI, S) declining at the top. The high concentration of carbonates could be connected with mineral spring activity rather than with the presence of molluscs, which are not abundant in these units (Šolcová et al., 2018). The concentration of elements such as Si, K and Rb, indicating detrital input (Kylander et al., 2011), is low, so we assume the existence of a fluvio-lacustrine environment.

Subsequently, ~ 8050 cal BP the valley was probably dammed by a travertine mound, which led to the interruption of fluvial/fluvio-lacustrine sediment deposition, to the formation of the lakes, and to the deposition of lake marl (units 5b and 5a). An increased presence of green algae and some aquatic molluscs in this period confirms the expansion of a shallow water body (Šolcová et al., 2018). In this context, the sedimentary environment is best interpreted as part of a 'travertine-depositing system' (Pentecost, 2005). the chemical record of lake sediments indicates minimum organic productivity and detrital input, and a high concentration of carbonates associated with mineral spring activity. The decrease of carbonates since ~ 7900 cal BP and the increase in Al, Si, K, Rb, Ti and Fe was probably caused by a decline in the number of events of increased detrital input. The most significant detrital input event, visible ~ 7500 and ~ 7350 cal BP, was simultaneous with a repeated temporary vanishing of green algae (Šolcová et al., 2018). Increased Si in this unit could be connected with a high abundance of diatoms (Fig. 3) (Peinerud, 2000). Increased Fe and Mn concentrations are generally used to reflect redox conditions; however, in this case they rather indicate a change of sediment source (c.f. Davison, 1993). According to the lithostratigraphy, the lake was formed several times during the Holocene. Similar geomorphological development happened earlier at the nearby Santovka-PB site (ca 1 km up-stream), where a shallow riverine lake associated with increased accumulation of travertine deposits, which may have dammed the stream, was formed during MIS 1 (Šolcová et al., 2020).

A significant short-lasting change in sedimentation style took place between ca 7350 and 7300 cal BP, when the organic layer composed of organic and calcareous laminae was formed. Increased organics (LOI), S and Fe indicate the occurrence of iron-sulfide formation typical for anoxic environments (Kienel et al., 2013), which could seasonally alternate with biochemical calcite laminae (c.f. Zolitschka et al., 2015). The process behind the onset of seasonal anoxic conditions remains unclear. It could be partly caused by a change of water regime associated with the disappearance of Búr brook and/or waning of the mineral spring. This change is connected to environmental change recorded in an age-depth model about 7300 cal BP, more likely relating to a shift in climatic conditions. It is

https://doi.org/10.5194/egusphere-2023-118
Preprint. Discussion started: 7 March 2023
© Author(s) 2023. CC BY 4.0 License.

connected also with a minor decline of some woodland species (*Quercus*, *Tilia*) and an expansion of herbs (Asteraceae) and local Cyperaceae. The insignificance of change in the palynological record reflects the wide ecology optimum of broadleaf trees such as *Corylus*, *Tilia* sp. and *Quercus* sp. (c.f. Šolcová et al., 2018).

The lake was later re-formed and sedimentation in the lake environment lasted until 6800 cal BP. Renewed production of the mineral spring is indicated by increased carbonates (Ca, Mg), but there is also a gradual increase of detrital material reflecting increasing erosion in the area. Environmental conditions in the lake were different compared to the previous lake phase (units 5b and 5a). The change is demonstrated by the different abundance and number of benthic organism species. Moreover, rafts had not yet occurred in any of the lithostratigraphic units (Fig. 3). Later (after 6800 cal BP), the lake deposits were overlaid by colluvial sediments accumulated probably in a water body, which is reflected by very high values of proxies of detrital input (Kylander et al., 2011) and the preservation of aquatic snails and green algaes (Šolcová et al., 2018). At the same time (after 6800 BP), a significant change of vegetation happened, when woodland vegetation was suppressed, while Poaceae and Cyperaceae expanded simultaneously with an increased presence of microcharcoals. This clearly indicates an increasing human impact in the Late Neolithic period (6850–6400 cal BP) in the surroundings (Šolcová et al., 2018).

5.2 $\delta^{18}O$ and $\delta^{13}C$ data interpretation

Values of $\delta^{18}O$ in the Santovka-village section (Fig. 4) possibly correspond to both travertine and tufa whereas positive $\delta^{13}C$ values correspond rather to values of thermogene travertines (c.f. Pentecost, 2005). Travertine deposits in the Santovka area were previously analysed at two other places. Values obtained from the main travertine mound of Pleistocene origin at the Santovka site with slightly lower values of $\delta^{18}O$ and higher values of $\delta^{13}C$ clearly correspond to thermogene travertines (Vieira et al., 2022). Such positive values of $\delta^{13}C$ in this period indicate a strong influence of marine bedrock sediments associated with deep water circulation (see Vieria et al., 2022) and/or dissolved pleistocene travertines. The nearby Santovka-PB section also provided positive $\delta^{13}C$ values attributed to the Late glacial and Pleniglacial record and a shift to negative values at the beginning of the Holocene (Šolcová et al., 2020), indicating a transition from travertines to tufas, unlike values for Holocene deposits at Santovka-village.

The ratios of stable carbon ($^{13}C/^{12}C$) and oxygen ($^{18}O/^{16}O$) isotopes in travertines *sensu lato* were possibly affected by the temperature of the water and eventually by the distance from the hot spring orifice, by kinetic effects related to isotope fractionation during travertine deposition, and also by diagenesis. The recent temperature in the nearest spring (core B3) is lower than 27°C (Bačová et al., 2016) and the waters of the former lake could have been supplied by the brook, so we conclude that mixed the water was close to ambient temperature, which is why the $\delta^{18}O$ record is more similar to riverine tufas. Riverine tufas specifically could reflect fractionation related to evaporation, CO_2

https://doi.org/10.5194/egusphere-2023-118
Preprint. Discussion started: 7 March 2023
© Author(s) 2023. CC BY 4.0 License.

degassing or metabolic consumption of lighter isotopes (Andrews, 2006; Gandin and Capezzuoli, 2008). Variations of $\delta^{18}O$ in the tufa could have been influenced mainly by the mean annual isotopic composition of the meteoric water at the time of calcite precipitation (Darling, 2004) resulting from the mean air temperature (Andrews et al., 1994; Janssen, 2000; Andrews, 2006) and the continentality effect (Andrews et al., 1994; Andrews, 2006), similarly to speleothems. However, climate-hydrology changes can cancel each other out due to variations in hydrology (McDermott, 2004; Fairchild et al., 2006; Lachniet, 2009).

Usually, the variability of $\delta^{13}C$ in freshwater carbonates is influenced by $\delta^{13}C$ values of the dissolved primary carbonates (Fairchild and Baker, 2012) and the origin of the CO_2 (Kele et al., 2011) which was originally dissolved in the precipitating water and could be inorganic (atmospheric, igneous, thermometamorphic, etc) as well as organic and connected with the type of vegetation and development (e.g. Dabkowski et al., 2019; Hercmann et al., 2020; Welte et al., 2021). Palynological studies of the area indicate a continuum habitats with open vegetation (e.g. Šolcová et al., 2018), so an increase of C4 plants is rather the result of local wetland vegetation changes than changes in the surrounding terrestrial vegetation, as has been described from mountain regions, for example the Low Tatras (c.f. Hercman et al., 2020). In the temperate climate zone, decreases of $\delta^{13}C$ in freshwater carbonates are connected with more productive vegetation and root respiration during wetter and warmer periods whereas higher $\delta^{13}C$ values during drier and colder periods are connected with reduced biological and pedological activity in soil (e.g. Deines, 1980; Surić et al., 2021).

In the Santovka-village record, we can clearly see an overall increasing trend of $\delta^{18}O$ during the mid-Holocene (Fig. 8). A similar trend of $\delta^{18}O$ increasing was identified in the Western Carpathians (Tatras) where speleothem of the Demänová cave system provided evidence of changes in seasonality of precipitation (Hercman et al., 2020). Increased values of $\delta^{18}O$ around ~ 8050–7900 cal BP, as well as in the Santovka-PB section (Šolcová et al., 2020), possibly reflect a short warm period in Central Europe, as suggested for Mondsee between 8100 and 8000 cal BP (Andersen et al., 2017). The Santovka $\delta^{13}C$ record indicates lasting dry conditions till ~ 7800 cal BP, similarly as in peat at Mohoş (Túri et al., 2021). Values of $\delta^{18}O$ are rather lower-than-average between ~ 7800 and ~ 7400 cal BP, which indicates lower temperatures, similarly to the Santovka-PB section and possibly to Katerloch cave (Boch et al., 2009) and Pál-völgyi cave (Demény et al., 2013). At Santovka-village, it is followed by a flip of both $\delta^{18}O$ and $\delta^{13}C$ isotopic records ~ 7400 cal BP. The abrupt increase of $\delta^{18}O$ is synchronous with the increase of $\delta^{18}O$ in Katerloch cave (Boch et al., 2009) and Pál-völgyi cave (Demény et al., 2013). We suppose an incorporation or *in situ* development of respired soil and decreased degassing (overall activity) of the spring aquifer, both possibly connected with drought. At the geographically near site Mituchovce (ca 100 km NW) a fairly similar trend of increasing $\delta^{13}C$ tillca 7350 ka BP was recorded (Dabkowski et al., 2019). Moreover, a similar drought and warm period in 7500–7400 cal BP was recently discovered in Grgosova cave (Surić et al., 2021). The subsequent opposite development of both isotopic records ~ 7300 BP was possibly caused by a return of warm and wet conditions on the one hand

https://doi.org/10.5194/egusphere-2023-118
Preprint. Discussion started: 7 March 2023
© Author(s) 2023. CC BY 4.0 License.

and/or a change of the lake environment associated with the development of the lake sediment (unit 3) on the other hand. This change might have been caused by deforestation (Dabkowski, 2014) of the area, but according to a palynological study there is no evidence of it in the Santovka-village section (c.f. Šolcová et al., 2018). Since ~ 7300 BP, $\delta^{18}O$ values indicate mild cooling, while $\delta^{13}C$ remains relatively low, which could reflect wetness or landscape change. However, this development is not recorded in such detail because of the lower deposition rate.

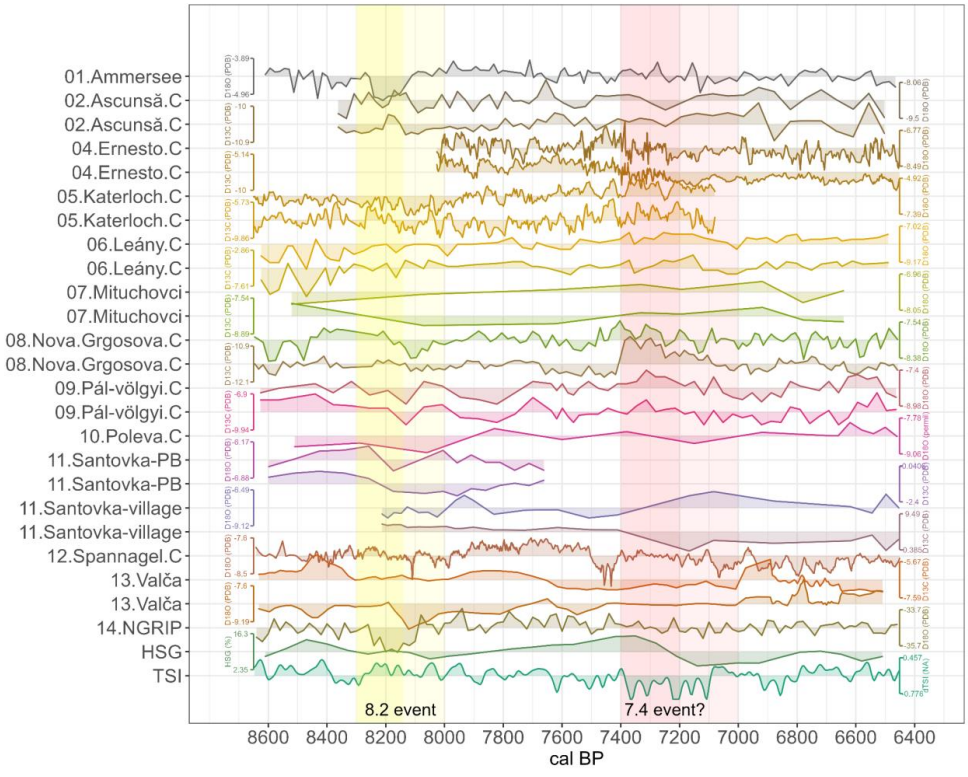

Fig. 8 Time series of climatic sensitive proxies ($\delta^{13}C$ and $\delta^{18}O$) from tufa deposits, speleothems, and lake and travertine lake sediments of Central, Central-Eastern and South-Eastern Europe compared with the North GRIP ice core record (bottom) (NGRIP Members, 2004). Labels on the left represent individual records/sites (.C means cave). Yellow bands define the 8.2 ka BP event (yellow = Rasmussen et al. 2014, light yellow = Weninger et al. 2006), and the red band defines the proposed 7.4 ka BP event (Surić et al., 2021). HSG = Hematite stained grains (Bond et al., 2001). TSI = Total solar irradiance (Steinhilber et al., 2009).

https://doi.org/10.5194/egusphere-2023-118
Preprint. Discussion started: 7 March 2023
© Author(s) 2023. CC BY 4.0 License.

5.3 Regional variability of climate development

The most prominent Holocene climatic fluctuation, referred to as the 8.2 ka BP event (~ 8300–8140 cal BP according to Rasmussen et al., 2014) has been described extensively in terms of its cause and consequences (e.g. Alley and Ágústsdóttir, 2005). We have detected a clearly related climate shift in the $\delta^{18}O$ record in Greenland NGRIP (NGRIP Members, 2004) about 8110–8060 cal BP as well as in Ammersee (Czymzik et al., 2013) about 8115–8065 cal BP. However, have not detected any significant climate shift in the $\delta^{18}O$ record of any of the Central-Eastern and South-Eastern Europe sites studied with the exception of Ascunsă (8003–7853 cal BP) and Poleva (8260–7910 cal BP) Caves. It appears that the detectShift method is effective in identifying shifts in means, but it may overlook minor fluctuations within a stationary series such as those observed around 8.2 ka BP in Katerloch, Nova Grgosova, and Valča. Our analysis suggests that these fluctuations may cause temporary deviations but do not alter the overall stationarity. The shift in Grgosova Cave was detected earlier (8508–8458), while minor dips related to the 8.2 ka BP event in other records were not substantial enough to be detected.. The signal of the 8.2 ka BP event in $\delta^{18}O$ records is indeed disputable in the Eastern and Southern Carpathians (Constantin et al., 2007; Drăguşin et al., 2014; Surić et al., 2021). There is, however, evidence of 8.4–8.2 ka BP shifts in $\delta^{13}C$ records of the Santovka-PB sequence (8412–8362 and 8312–8262 cal BP), Pál-völgyi (8463—8213 cal BP) and Leány (8340–8140 cal BP) and Ascunsă (8353–8303 cal BP) Caves in the northern Pannonian Basin (Table 3). The surprising timing preceding the conventional span of the 8.2 event could be associated with an abrupt decrease in total solar irradiance (TSI; Fig. 8). The Santovka-village $\delta^{18}O$ shift period (7404–7204 cal BP) does not overlap with shifts detected in other $\delta^{18}O$ records with the exceptions of the Grotta di Ernestoa (7252–7202 cal BP), the Pál-völgyi Cave (7313–7263 cal BP) and the Spannagel Cave (7551–7451 cal BP) (Table 3). Similarly, an even more significant abrupt shift was detected in the $\delta^{13}C$ records of Santovka-village (7304–7254 cal BP), Grotta di Ernesto (7402–7352 cal BP), Katerloch Cave (7580–7480 cal BP), Poleva Cave (7510–7410 cal BP) and Nova Grgosova Cave (7458–7408 cal BP), where a synchronous event was identified and discussed in a previous study (Surić et al., 2021). Palaeolimnological records and peat records from Carpathians do not indicate the occurrence of the 7.4 ka BP event (Túri et al., 2021; Feurdean et al., 2007; Magyari et al., 2014). Nevertheless, at Sfânta Ana in the Eastern Carpathians (Romania) a long-term rise of humidity after 7.4 ka BP is indicated palynologically (Magyari et al., 2014).

The regional evidence of climate shifts around 7.4 ka BP could possibly be explained by the development of atmospheric circulation in the mid-Holocene. Central Europe is situated at the transition between the warm temperate fully humid zone (West) and the boreal fully humid zone with warm summers (East) (Kottek et al., 2006), so it is sensitive to changes in air circulation. The supposed mechanism behind the decline of humid westerlies in Central Europe is atmospheric blocking over Western Europe, connected with a low East Atlantic index (e.g. Moore et al., 2013). Therefore it is a

https://doi.org/10.5194/egusphere-2023-118
Preprint. Discussion started: 7 March 2023
© Author(s) 2023. CC BY 4.0 License.

subject of discussion whether changes in atmospheric circulation could be reflected in the Holocene palaeoclimate record in Central-Eastern Europe. Generally, an increasing trend of $\delta^{18}O$ during the mid-Holocene is apparent in the Santovka-village record (Fig. 8), similarly to most reference records with the exceptions of Leány, Nova Grgosova Cave and Spannagel Cave, where there is an opposite trend. It has been noted that Mediterranean and Balkan $\delta^{18}O$ values are connected with a change of precipitation and that decreasing values are connected to wetter periods (Bar-Matthews et al., 2004; Drăguşin et al., 2014; Surić et al., 2021). It has also been argued that water was possibly transported more frequentely from the Mediterranean and Black Sea regions during the early Holocene and at the beginning of the mid-Holocene whereas the rest of the mid and in late Holocene was connected with an increased role of westerlies (Hermcan et al., 2020). A recently published model of mid-Holocene summer temperatures indicates a strong spatial dependence of summer near-surface temperatures on soil moisture, increasing towards Eastern Europe and the Mediterranean region and reaching a maximum in the area north of the Black Sea (Russo et al., 2022). The problem of regional discrepancies in reconstructed annual temperatures was recently explained by the Arctic amplification and seasonal sea ice loss, which caused an increase of mid- and high-latitude temperatures (Park et al., 2019). From the global perspective the 7.4–7.0 ka BP period is associated with peaking and, consequently, with declining petrological tracers of drift ice in the North Atlantic (not labeled as separate Bond event) synchronous with a local peak and a consequent decrease of TSI (Fig. 8; c.f. Bond et al., 2001; Steinhilber et al., 2009).

https://doi.org/10.5194/egusphere-2023-118
Preprint. Discussion started: 7 March 2023
© Author(s) 2023. CC BY 4.0 License.

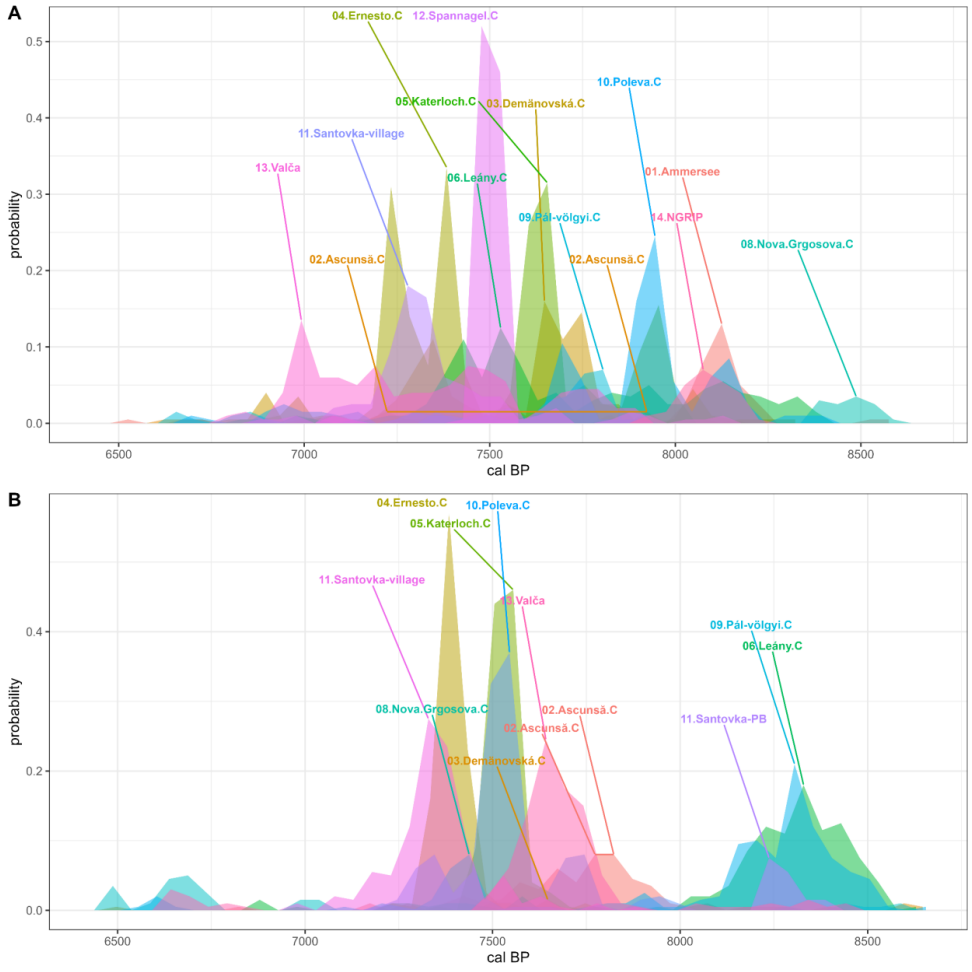

525 Fig. 9) Summary probabilities for different records (distinguished by colors) obtained using the detectShift function (actR library) for D18O (case A) and D13C (case B).

6. Conclusion

The sedimentary infill of a small valley dammed by travertine at the Santovka site allowed us to perform
530 an age-ensembled reconstruction of the local sedimentary environment. It has been argued that the $\delta^{18}O$ and $\delta^{13}C$ signal in the sediments bears information about the mean annual isotopic composition of the meteoric water despite the presence of mineral and thermal springs, so it reflects the palaeoclimatic record. The fluvial/fluvio-lacustrine sediments accumulated on the valley bottom till ca 8050, when the sedimentary environment changed into a travertine lake represented by lake marl deposits. The $\delta^{18}O$
535 values are low until this period, similarly to the Santovka-PB section with no significant climate shift in the $\delta^{18}O$ record synchronous with 8.2 ka BP. However, a $\delta^{13}C$ shift was detected around 8.3 ka BP in the Santovka-PB sequence. The calcareous lake marl accumulation was interrupted about cca 7350–

https://doi.org/10.5194/egusphere-2023-118
Preprint. Discussion started: 7 March 2023
© Author(s) 2023. CC BY 4.0 License.

7300, when the lake dried out and deposition of an organic layer took place. An abrupt short-lasting drought is reflected also by an abrupt decline of $\delta^{13}C$. A similar synchronous dip associated with drought has so far been identified in only one speleothem record (Nova Grgosova Cave, Croatia). Whereas the 8.2 ka BP event (clearly identified in the $\delta^{18}O$ records of Greenland ice core and Central European lake sediments) is insignificant in most Central-Eastern and South-Eastern European records, the short-lasting drought 7350–7300 ka BP from Santovka is synchronous with climate shifts detected ~ 7.5–7.2 ka BP in $\delta^{13}C$ records of most of the reference sites. The overall mid-Holocene trend, observed in most of the archives studied, is an increase of $\delta^{18}O$ values. All findings indicate a change in temperatures and humidity and/or a change in the circulation of air masses in Central-Eastern and South-Eastern Europe. Therefore, these regions were possibly influenced by circulation from the Eastern Mediterranean in the mid-Holocene. Future research could examine the impact of these climate shifts on the last hunter-gatherers and the first farmers in the context of spreading agriculture in Europe.

Appendices

Appendix is available here: 10.5281/zenodo.7582204

Table S1 is attached as supplementary material

Code availability

Code is included in Appendix available here: 10.5281/zenodo.7582204

Data availability

The data are available in the attached files.

Author contributions

Jan Petřík: Investigation, Funding acquisition, Conceptualization, Writing – original draft preparation, Formal analysis, Software, Methodology, Visualization

Katarína Adameková: Writing – original draft preparation, prepared the manuscript with contributions from all co-authors, Visualization, Conceptualization

Sándor Kele: Writing – review & editing, Supervision

Rastislav Milovský: Formal analysis

Libor Petr: Investigation, Writing – original draft preparation

Petr Tóth: Investigation, Funding acquisition, Visualization

Nicholas McKay: Methodology, Software, developed the model code and performed the simulations.

Competing interests

The authors declare that they have no conflict of interest.

https://doi.org/10.5194/egusphere-2023-118
Preprint. Discussion started: 7 March 2023
© Author(s) 2023. CC BY 4.0 License.

Acknowledgments

The work towards the results presented here was supported by the Czech Science Foundation (project Tracing the Neolithic transition through the first pottery GA20-19542S). The authors thank Juraj Lauko and Jozef Bátora.

References

Adameková, K. and Petřík, J.: The myth of 'Bohunician soil': a re-evaluation of the MIS 3 palaeosol record at the Brno-Bohunice site (Czechia), CATENA, 217, 106510, https://doi.org/10.1016/j.catena.2022.106510, 2022.

Alley, R. B. and Ágústsdóttir, A. M..: The 8k event: cause and consequences of a major Holocene abrupt climate change, Quaternary Science Reviews, 24, 10–11, https://doi.org/10.1016/j.quascirev.2004.12.004, 2005.

Andrews, J. E.: Palaeoclimatic records from stable isotopes in riverine tufas: synthesis and review, Earth-Science Reviews, 75 (1–4), 85–104, https://doi.org/10.1016/j.earscirev.2005.08.002, 2006.

Andrews, J. E., Pedley, H.M. and Dennis, P. F.: Stable isotope record of palaeoclimatic change in a British Holocene tufa, The Holocene, 4 (4), 349–355, https://doi.org/10.1177/095968369400400402, 1994.

Andersen, N., Lauterbach, S., Erlenkeuser, H., Danielopol, D. L., Namiotko, T., Hüls, M., Belmecheri, S., Dulski, P., Nantke, C., Meyer, H., Chapligin, B., on Grafenstein, U. and Brauer, A.: Evidence for higher-than-average air temperatures after the 8.2 ka event provided by a Central European δ18O record, Quaternary Science Reviews, 172, 96–108, https://doi.org/10.1016/j.quascirev.2017.08.001, 2017.

Bačová, N., Németh, Z. and Repčiak, M.: Mineral Waters of the Dudince Spa, Slovak Geological Magazine, 16 (2), 125–147, 2016.

Bačová, N., Ženišová, Z. and Michalko, J.: Chemické zloženie minerálnych vôd Dudiniec, Santovky a Slatiny, Podzemná voda, 21 (2), 63–82, 2015.

Bar-Matthews, M. and Ayalon, A.: Speleothems as palaeoclimate indicators, a case study from Soreq Cave located in the Eastern Mediterranean Region, Israel, in: Past Climate Variability through Europe and Africa. Developments in Paleoenvironmental Research, vol 6. edited by: Battarbee, R.W., Gasse, F. and Stickley, C.E., Springer, Dordrecht, Netherlands, 363–391, https://doi.org/10.1007/978-1-4020-2121-3_18, 2004.

https://doi.org/10.5194/egusphere-2023-118
Preprint. Discussion started: 7 March 2023
© Author(s) 2023. CC BY 4.0 License.

Blaauw, M., Andres Christen, J. and Aquino Lopez, M. A.: Rbacon: Age-Depth Modelling using Bayesian Statistics. R package version 2.5.8. https://CRAN.R-project.org/package=rbacon, 2022.

Bond, G., Kromer, B., Beer, J., Muscheler, R., Evans, M. N., Showers, W., Hoffmann, S., Lotti-bond, R., Hajdas, I. and Bonani. G.: Persistent Solar Influence on North Atlantic Climate During the Holocene, Science, 294 (5549), 2130–2136. DOI: 10.1126/science.1065680, 2001.

Boch, R., Spötl, C. and Kramers, J.: High-resolution isotope records of early Holocene rapid climate change from two coeval stalagmites of Katerloch Cave, Austria, Quaternary Science Reviews, 28 (23–24), 2527–2538, https://doi.org/10.1016/j.quascirev.2009.05.015, 2009.

Capezzuoli, E., Gandin, A. and Pedley, M.: Decoding tufa and travertine (fresh water carbonates) in the sedimentary record: The state of the art, Sedimentology, 61, 1–21, https://doi.org/10.1111/sed.12075, 2014.

CGIAR CSI: https://srtm.csi.cgiar.org/, last access: 17 January 2023.

Constantin, S., Bojar, A. V., Lauritzen, S. E. and Lundberg, J.: Holocene and Late Pleistocene climate in the sub-Mediterranean continental environment: A speleothem record from Poleva Cave (Southern Carpathians, Romania), Palaeogeography, Palaeoclimatology, Palaeoecology, 243 (3–4), 322–338, https://doi.org/10.1016/j.palaeo.2006.08.001, 2007.

Czymzik, M., Brauer, A., Dulski, P., Plessen, B., Naumann, R., von Grafenstein, U. and Scheffler, R.: Orbital and solar forcing of shifts in Mid- to Late Holocene flood intensity from varved sediments of pre-alpine Lake Ammersee (southern Germany), Quaternary Science Reviews, 61, 96–110, https://doi.org/10.1016/j.quascirev.2012.11.010., 2013.

Dabkowski, J.: High potential of calcareous tufas for integrative multidisciplinary studies and prospects for archaeology in Europe, Journal of Archaeological Science, 52, 72–83, https://doi.org/10.1016/j.jas.2014.07.013, 2014.

Dabkowski, J., Frodlová, J., Hájek, M., Hájková, P., Petr, L., Fiorillo, D., Dudová, L. and Horsák, M.: A complete Holocene climate and environment record for the Western Carpathians (Slovakia) derived from a tufa deposit, The Holocene, 29 (3), 493–504, https://doi.org/10.1177/0959683618816443, 2019.

Darling, W.G.: Hydrological factors in the interpretation of stable isotopic proxy data present and past: a European perspective, Quaternary Science Reviews, 23 (7–8), 743–770, https://doi.org/10.1016/j.quascirev.2003.06.016, 2004.

Davison, W.: Iron and manganese in lakes, Earth-Science Review, 34, 119–163, https://doi.org/10.1016/0012-8252(93)90029-7, 1993.

https://doi.org/10.5194/egusphere-2023-118
Preprint. Discussion started: 7 March 2023
© Author(s) 2023. CC BY 4.0 License.

Deines, P.: The isotopic composition of reduced organic carbon. in: Handbook of Environmental Isotope Geochemistry, edited by: Fritz, P. and Fontes, J. C., Elsevier, Amsterdam, Netherlands, 329–406, 1980.

Demény, A., Czuppon, G., Siklósy, Z., Leél-Őssy, S., Lin, K., Shen, Ch-Ch. and Gulyás, K.: Mid-Holocene climate conditions and moisture source variations based on stable H, C and O isotope compositions of speleothems in Hungary, Quaternary International, 293, 150–156, https://doi.org/10.1016/j.quaint.2012.05.035, 2013.

Demény, A., Kern, Z, Hatvani, I. G., Torma, C., Topál, D., Frisia, S., Leél-Őssy, S., Czuppon, G. and Surányi, G.: Holocene hydrological changes in Europe and the role of the North Atlantic ocean circulation from a speleothem perspective, Quaternary International, 571, 1–10, https://doi.org/10.1016/j.quaint.2020.10.061, 2021.

Demovic, R., Hoefs, J. and Wedepohl, K.H.: Geochemische Untersuchungen an Travertinen der Slowakei, Contributions to Mineralogy and Petrology, 37, 15–28. https://doi.org/10.1007/BF00377303, 1972.

Divíšek, J., Hájek, M., Jamrichová, E., Petr, L., Večeřa, M., Tichý, L., Willner, W. and Horsák, M.: Holocene matters: Landscape history accounts for current species richness of vascular plants in forests and grasslands of eastern Central Europe, Journal of Biogeography, 47 (3), 721–735, https://doi.org/10.1111/jbi.13787, 2020.

Dobrowolski, R., Durakiewicz, T. and Pazdur, A.: Calcareous tufas in the soligenous mires of eastern Poland as an indicator of the Holocene climatic changes, Acta Geologica Polonica, 52 (1), 63–73, 2002.

Drăguşin, V., Staubwasser, M., Hoffmann, D. L., Ersek, V., Onac, B. P., and Veres, D.: Constraining Holocene hydrological changes in the Carpathian–Balkan region using speleothem $\delta^{18}O$ and pollen-based temperature reconstructions, Climate of the Past, 10, 1363–1380, https://doi.org/10.5194/cp-10-1363-2014, 2014.

Fairchild, I. J., Smith, C. L., Baker, A., Fuller, L., Spötl, C., Mattey, D., McDermott, F., and E. I. M. F.: Modification and preservation of environmental signals in speleothems, Earth-Science Reviews, 75, 105–153, 2006.

Fairchild, I. J. and Baker, A. (Eds.): Speleothem science: from process to past environments, Wiley-Blackwell, Hoboken, New Jersey, United States, 448 pp., ISBN 978–1–405–19620–8, 2012.

Feurdean, A., Wohlfarth, B., Björkman, L., Tantau, I., Bennike, O., Willis, K.J., Farcas, S. and Robertsson, A.M.: The influence of refugial population on Lateglacial and early Holocene vegetational changes in Romania, Review of Palaeobotany and Palynology, 145, 305–320, 2007.

https://doi.org/10.5194/egusphere-2023-118
Preprint. Discussion started: 7 March 2023
© Author(s) 2023. CC BY 4.0 License.

Fohlmeister, J., Vollweiler, N., Spötl, C. and Mangini, A.: COMNISPA II: Update of a mid-European isotope climate record, 11 ka to present, The Holocene, 23 (5), 749–754, https://doi.org/10.1177/0959683612465446, 2013.

Franko, O., Remšík, A. and Fendek, M. (Eds.): Atlas geotermálnej energie Slovenska, Geologický ústav Dioníza Štúra, Bratislava, Slovakia, 164 pp., ISBN 80–85314–38–X, 1995.

Gandin, A., and Capezzuoli, E.: Travertine versus Calcareous Tufa: Distinctive Petrologic Features and Stable Isotope Signature, Il Quaternario. Italian Journal of Quaternary Sciences, 21, 125–136, 2008.

Gradzinski, M., Dulinski, M., Hercman, H., Stworzewicz, E., Holúbek, P., Rajnoga, P., Wróblewski, W. and Kovácová, M.,: Facies and age of travertines from Spis and Liptov regions (Slovakia) – Preliminary results, Slovenský Kras (Acta Carsologica Slovaca), 46/1, 31–40, 2008.

Hercman, H., Gąsiorowski, M., Pawlak, J., Błaszczyk, M., Gradziński, M., Matoušková, Š., Zawidzki, P., and Bella, P.: Atmospheric circulation and the differentiation of precipitation sources during the Holocene inferred from five stalagmite records from Demänová Cave System (Central Europe), The Holocene, 30 (6), 834–846, https://doi.org/10.1177/0959683620902224, 2020.

Holko, L., Dóša, M., Michalko, J. and Šanda, M.:Isotopes of oxygen-18 and deuterium in precipitation in Slovakia, Journal of Hydrology and Hydromechanics, 60 (4), 265–276, https://doi.org/10.2478/v10098-012-0023-2, 2012.

Hók, J., Šujan, M., Sýkora, M. and Šipka, F.: Geológia a tektonika levicko-santovskej elevácie (juhozápadný okraj štiavnického stratovulkánu), Geologické práce, Správy, 135, 47–50, 2020.

Jamrichová, E., Petr, L., Jiménez-Alfaro, B., Jankovská, V., Dudová, L., Pokorný, P., Kołaczek, P., Zernitskaya, V., Čierniková, M., Břízová, E., Syrovátka, V., Hájková, P. and Hájek M.: Pollen-inferred millennial changes in landscape patterns at a major biogeographical interface within Europe, Journal of Biogeography, 44 (10), 2386–2397, https://doi.org/10.1111/jbi.13038, 2017.

Janssen, A.: Petrography and Geochemistry of Active and Fossil Tufa Deposits from Belgium, Ph.D. thesis, Katholieke Universiteit, Leuven, Belgium, 329 pp., 2000.

Juřičková, L., Pokorný, P., Hošek, J., Horáčková, J., Květoň, J., Zahajská, P., Jansová, A., Ložek, V.: 2018. Early postglacial recolonisation, refugial dynamics and the origin of a major biodiversity hotspot. A case study from the Malá Fatra mountains, Western Carpathians, Slovakia. The Holocene 28 (4), 583–594.https://doi.org/10.1177/0959683617735592

Kele, S.: Édesvízi mészkövek vizsgálata a Kárpát-medencéből: paleoklimatológiai és szedimentológiai elemzések (Investigations on freshwater limestones from the Carpathian-basin: paleoclimatological and sedimentological studies), Ph.D. thesis, Eötvös Loránd Tudományegyetem, Hungaria, 176 pp., 2009.

https://doi.org/10.5194/egusphere-2023-118
Preprint. Discussion started: 7 March 2023
© Author(s) 2023. CC BY 4.0 License.

Kele, S., Korpás, L., Demény, A., Kovács-Pálffy, P., Bajnóczi, B. and Medzihradszky, Z.: Paleoenvironmental evaluation of the Tata Travertine Complex (Hungary), based on stable isotopic and petrographic studies, Acta Geologica Hungarica, 49 (1), 1–31, https://doi.org/10.1556/ageol.49.2006.1.1, 2006.

Kele, S., Özkul, M., Gökgöz, A., Fórizs, I., Baykara M. O., Alcicek, M. C. and Németh, T.: Stable isotope geochemical and facies study of Pamukkale travertines: new evidences of lowtemperature non-equilibrium calcite–water fractionation, Sedimentary Geology, 238 (1–2), 191–212, https://doi.org/10.1016/j.sedgeo.2011.04.015, 2011.

Kienel, U., Dulski, P., Ott, F., Lorenz, S. and Brauer, A.: Recently induced anoxia leading to the preservation of seasonal laminae in two NE-German lakes, Journal of Paleolimnology, 50, 535–544. https://link.springer.com/article/10.1007/s10933-013-9745-3, 2013.

Konečný, V. (Ed.): The geological map of Štiavnica mountains and Pohronský Inovec (Štiavnický stratovulkán) (in Slovak), Ministerstvo životného prostredia SR - Geologická služba SR, Bratislava, Slovakia, Map 1 : 50 000, 1998.

Kottek, M., Grieser, J., Beck, C., Rudolf, B. and Rubel, F.: World Map of the Köppen-Geiger climate classification updated, Meteorologische Zeitschrift, 15 (3), 259–263, DOI: 10.1127/0941-2948/2006/0130, 2006.

Kylander, M. E., Ampel, L., Wohlfarth, B. and Veres, D.:High-resolution X-ray fluorescence core scanning analysis of Les Echets (France) sedimentary sequence: new insights from chemical proxies, journal of Quaternary Science, 26 (1), 109–117, https://doi.org/10.1002/jqs.1438, 2011.

Lachniet, M. S.: Climatic and environmental controls on speleothem oxygen-isotope values, Quaternary Science Reviews, 28 (5–6), 412–432 https://doi.org/10.1016/j.quascirev.2008.10.021, 2009.

Maglay, J. (Ed.): Quaternary geological map of Slovakia – Quaternary genetical (deposits) types, Štátny geologický ústav Dionýza Štúra, Bratislava, Slovakia, Map 1 : 500 000, 2009.

Magyari, E.K., Veres, D., Wennrich,V., Wagner, B., Braun, M., Jakab, G., Karátson, D., Pál, Z., Ferenczy, Gy, St-Onge, G., Rethemeyer, J., Francois, J.-P. , von Reumont, F. and Schäbitz, F.: Vegetation and environmental responses to climate forcing during the Last Glacial Maximum and deglaciation in the East Carpathians: attenuated response to maximum cooling and increased biomass burning, Quaternary Science Reviews, 106, 278–298, https://doi.org/10.1016/j.quascirev.2014.09.015, 2014.

https://doi.org/10.5194/egusphere-2023-118
Preprint. Discussion started: 7 March 2023
© Author(s) 2023. CC BY 4.0 License.

Maps Arcanum: https://maps.arcanum.com/en/map/europe-19century-secondsurvey, last access: 16 January 2023.

Mazúr, E. and Lukniš, M.: Regionálne geomorfologické členenie SSR, Geografický časopis, 30 (2), 101–125, 1986.

McDermott, F.: Paleo-climate reconstruction from stable isotope variations in speleothems: A review, Quaternary Science Reviews, 23, (7–8), 901–918., https://doi.org/10.1016/j.quascirev.2003.06.021, 2004.

McKay, N. P. and Emile-Geay, J.: Technical note: The Linked Paleo Data framework – a common tongue for paleoclimatology, Climate of the Past, 12, 1093–1100, https://doi.org/10.5194/cp-12-1093-2016, 2016.

McKay, N. P., Emile-Geay, J. and Khider, D.: GeoChronR – an R package to model, analyze, and visualize age-uncertain data, Geochronology, 3, 149–169, https://doi.org/10.5194/gchron-3-149-2021, 2021.

McKay, N. P. and Emile-Geay, J.: The Abrupt Change Toolkit in R (v0.1.3), Zenodo [code], https://doi.org/10.5281/zenodo.6926613, 2022.

Miclós, L.: Atlas krajiny Slovenskej republiky, Ministerstvo životného prostredia SR, Bratislava, Slovakia, 342 pp., ISBN 80–88833–27–2, 2002, 2013.

Moore, G. W. K., Renfrew, I. A., & Pickart, R. S.: Multidecadal mobility of the North Atlantic Oscillation. Journal of Climate, 26(8), 2453–2466. https://doi.org/10.1175/JCLI-D-12-00023.1

Natural Earth Data: https://www.naturalearthdata.com/, last acces: 17 January 2023.

North Greenland Ice Core Project NGRIP Members.: High-resolution record of Northern Hemisphere climate extending into the last interglacial period, Nature, 431, 147–151. https://doi.org/10.1038/nature02805, 2004.

Park, H. S., Kim, S. J., Stewart, A. L., Son, S. W. and Seo, K. H.: Mid-Holocene Northern Hemisphere warming driven by Arctic amplification, Science Advances, 5 (12), eaax8203, https://www.science.org/doi/10.1126/sciadv.aax8203, 2019.

Peinerud, E. K.: Interpretation of Si concentrations in lake sediments: three case studies, Environmental Geology, 40, 64–72. https://doi.org/10.1007/PL00013330, 2000.

https://doi.org/10.5194/egusphere-2023-118
Preprint. Discussion started: 7 March 2023
© Author(s) 2023. CC BY 4.0 License.

Pazdur, A., Dobrowolski, R., Durakiewicz, T., Piotrowska, N., Mohanti, M. and Das, S.: δ13C and δ18O time record and palaeoclimatic implications of the Holocene calcareous tufa from Poland and India (Orissa), Geochronometria, 21, 97–108, 2002.

Pentecost, A.: Travertine, Springer, Amsterdam, Netherlands, 448 pp., ISBN 978–1–4020–3606–4, 2005.

Pivko, D. and Vojtko, R.: A review of travertines and tufas in Slovakia: Geomorphology, environments, tectonic pattern, and age distribution, Acta Geologica Slovaca, 13 (1), 49–78, 2021.

Rasmussen, S. O., Bigler, M., Blockley, S. P., Blunier, T., Buchardt, S. L., Clausen, H. B., Cvijanovic, I., Dahl-Jensen, D., Johnsen, S. J., Fischer, H., Gkinis, V., Guillevic, M., Hoek, W. Z., Lowe, J. J., Pedro, J. B., Popp, T., Seierstad, I. K., Steffensen, J. P., Svensson, A. M., Vallelonga, P., Vinther, B. M., Walker, M. J. C., Wheatley, J. J. and Winstrup, M.: A stratigraphic framework for abrupt climatic changes during the Last Glacial period based on three synchronized Greenland ice-core records: refining and extending the INTIMATE event stratigraphy, Quaternary Science Reviews, 106, 14–28, https://doi.org/10.1016/j.quascirev.2014.09.007, 2014.

Reimer, P. J., Austin, W. E. N., Bard, E., Bayliss, A., Blackwell, P. G., Bronk Ramsey, C., Butzin, M., Cheng. H., Edwards, R. L., Friedrich, M., Grootes, P. M., Guilderson, T. P., Hajdas, I., Heaton, T. J., Hogg, A. G., Hughen, K. A., Kromer, B., Manning, S. W., Muscheler, R., Palmer, J. G., Pearson, C., van der Plicht, J., Reimer, R. W., Richards, D. A., Scott, E. M., Southon, J. R., Turney, C. S. M., Wacker, L., Adolphi, F., Büntgen, U., Capano, M., Fahrni, S. M., Fogtmann-Schulz, A., Friedrich, R., Köhler, P., Kudsk, S., Miyake, F., Olsen, J., Reinig, F., Sakamoto, M., Sookdeo, A. and Talamo, S.: The IntCal20 Northern Hemisphere Radiocarbon Age Calibration Curve (0–55 cal kBP), Radiocarbon, 62 (4), 725–757, https://doi.org/10.1017/RDC.2020.41, 2020.

Rohling, E. J. and Pälike, H.: Centennial-scale climate cooling with a sudden cold event around 8,200 years ago, Nature, 434, 975–979, https://doi.org/10.1038/nature03421, 2005.

Russo, E., Fallah, B., Ludwig, P., Karremann, M. and Raible, C. C.: The long-standing dilemma of European summer temperatures at the mid-Holocene and other considerations on learning from the past for the future using a regional climate model, Climate of the Past, 18, 895–909, https://cp.copernicus.org/articles/18/895/2022/cp-18-895-2022.pdf, 2022.

Scholz, D., Frisia, S., Borsato, A., Spotl, C., Fohlmeister, J., Mudelsee, M., Miorandi, R. and Mangini, A.: Holocene climate variability in north-eastern Italy: potential influence of the NAO and solar activity recorded by speleothem data, Climate of the Past, 8, 1367–1383, https://doi.org/10.5194/cp-8-1367-2012, 2012.

https://doi.org/10.5194/egusphere-2023-118
Preprint. Discussion started: 7 March 2023
© Author(s) 2023. CC BY 4.0 License.

SGUDS: https://ags.geology.sk/arcgis/services/WebServices/GM50/MapServer/WMSServer, last acces: 15 August 2023.

Steinhilber, F., Beer, J. and Fröhlich, C.: Total solar irradiance during the Holocene, Geophysical Research Letters, 36 (19), L19704, https://doi.org/10.1029/2009GL040142, 2009.

Stoops, G.: Guidelines for Analysis and Description of Soil and Regolith thin Sections Soil Science, Society of America, Madison, United States, 184 pp., ISBN 0891188428, 2003.

Surić, M., Columbu, A., Lončarić, R., Bajo, P., Bočić, N., Lončar, N., Drysdale, R. N. and Hellstrom, J. C.: Holocene hydroclimate changes in continental Croatia recorded in speleothem δ13C and δ18O from Nova Grgosova Cave, The Holocene, 31 (9), 1401–1416, https://doi.org/10.1177/09596836211019120, 2021.

Šolcová, A., Petr, L., Hájková, P., Petřík, J., Tóth, P., Rohovec, J., Bátore, J. and Horsák, M.: Early and middle Holocene ecosystem changes at the Western Carpathian/Pannonian border driven by climate and Neolithic impact, Boreas, 47 (3), 897–909, https://doi.org/10.1111/bor.12309, 2018.

Šolcová, A., Jamrichová, E., Horsák, M., Pařil, P., Petr, L., Heiri, O., Květoň, J., Křížek, M., Hartvich, F., Hájek, M. and Hájková, P.: Abrupt vegetation and environmental change since the MIS 2: a unique paleorecord from Slovakia (Central Europe), Quaternary Science Reviews, 230, 106170, https://doi.org/10.1016/j.quascirev.2020.106170, 2020.

Tămaş, T., Onac, B.P. and Bojar, A.V.: Late Glacial-Middle Holocene stable isotope records in two coeval stalagmites from the Bihor Mountains, NW Romania, Geological Quarterly, 49 (2), 185–194, 2005.

Tóth, P., Petřík, J., Bickle, P., Adameková, K., Denis, S., Slavíček, K., Petr., L., Pokutta, D. and Isaksson, S.: Radiocarbon dating of grass-tempered ceramic reveals the earliest pottery from Slovakia predates the arrival of farming, in preparation.

Túri, M., Hubay, K., Molnár, M., Braun, M., László, E., Futó, I. and Palcsuet, L.: Holocene paleoclimate inferred from stable isotope (δ18O and δ13C) values in Sphagnum cellulose, Mohos peat bog, Romania, Journal of Paleolimnology, 66, 229–248, https://doi.org/10.1007/s10933-021-00202-z, 2021.

Vieira, D., Rinyu, L. and Kele, S.: Stable and clumped isotope characterization of travertine spring mounds from Santovka and Dudince (Southern Slovakia), in: The 24th EGU General Assembly, Wien, Austria, 23–27 May 2022, EGU-7556, 2022).

Walker, M., Head, M. J., Berkelhammer, M., Björck, S., Cheng, H. , Cwynar, L., Fisher, D., Gkinis, V. Long, A., Lowe, J., Newnham, R., Rasmussen, S. and Weiss, H.: Formal ratification of the subdivision of the Holocene Series/Epoch (Quaternary System/Period): two new Global Boundary

https://doi.org/10.5194/egusphere-2023-118
Preprint. Discussion started: 7 March 2023
© Author(s) 2023. CC BY 4.0 License.

Stratotype Sections and Points (GSSPs) and three new stages/subseries, Episodes, 41 (4), 213–223, https://doi.org/10.18814/epiiugs/2018/0180162018, 2018.

Walker, M., Head, M. J., Berkelhammer, M., Björck, S., Cheng, H. , Cwynar, L., Fisher, D., Gkinis, V. Long, A., Lowe, J., Newnham, R., Rasmussen, S. and Weiss, H.: Subdividing the Holocene Series/Epoch: formalisation of stages/ages and subseries/subepochs, and designation of GSSPs and auxiliary stratotypes, Journal of Quaternary Science, 34 (3), 173–186, https://doi.org/10.1002/jqs.3097, 2019.

Welte, C., Fohlmeister, J., Wertnik, M., Wacker, L., Hattendorf, B., Eglinton, T. I., and Spötl, C.: Climatic variations during the Holocene inferred from radiocarbon and stable carbon isotopes in speleothems from a high-alpine cave, Climate of the Past, 17, 2165–2177, https://doi.org/10.5194/cp-17-2165-2021, 2021.

Weninger, B., Alram-Stern, E., Bauer, E., Clare, L., Danzeglocke, U., Jöris, O., Kubatzkie, C., Rollefsonf, G., Todorovag, H. and Van Andel, T.: Climate Forcing Due to the 8200 Cal yr BP Event Observed at Early Neolithic Sites in the Eastern Mediterranean, Quaternary Research, 66 (3), 401–420, https://doi.org/10.1016/j.yqres.2006.06.009, 2006.

ZBGIS: https://zbgis.skgeodesy.sk/mkzbgis/sk/zakladna-mapa, last acces: 15 August 2023.

Zolitschka, B., Francus, P., Ojala, A. E. K. and Schimmelmann, A.: Varves in lake sediments – a review, Quaternary Science Reviews, 117, 1–41, https://doi.org/10.1016/j.quascirev.2015.03.019, 2015.

Žák, K., Hladíková, J., Buzek, F., Kadlecová, R., Ložek, V., Cílek, V., Kadlec, J., Žigová, A., Bruthans, J. and Šťastný, M.: Special Papers No. 13, Czech Geological Survey, Praha, Czech Republic, 135 pp., ISBN 80–7075–472–9, 2001.